Progress in Oceanography 195 (2021) 102591

Contents lists available at ScienceDirect

Progress in Oceanography

journal homepage: www.elsevier.com/locate/pocean

Abyssal fauna, benthic microbes, and organic matter quality across a range of trophic conditions in the western Pacific ocean

Hidetaka Nomaki [a,*], Eugenio Rastelli [b], Andreia Alves [c], Hisami Suga [d], Sandra Ramos [c], Tomo Kitahashi [e], Masashi Tsuchiya [e], Nanako O. Ogawa [d], Yohei Matsui [a], Koji Seike [f], Norio Miyamoto [a], Cinzia Corinaldesi [g], Elisabetta Manea [h], Naohiko Ohkouchi [d], Roberto Danovaro [i,j], Takuro Nunoura [k], Teresa Amaro [l,m]

[a] X-star, Japan Agency for Marine-Earth Science and Technology (JAMSTEC), 2-15 Natsushima-cho, Yokosuka 237-0061, Japan
[b] Department of Marine Biotechnology, Stazione Zoologica Anton Dohrn, Fano Marine Centre, Viale Adriatico 1-N, 61032 Fano, Italy
[c] Interdisciplinary Centre of Marine and Environmental Research (CIIMAR/CIMAR), University of Porto (U.Porto), Av. General Norton de Matos s/n, 4450-208 Matosinhos, Portugal
[d] Research Institute for Marine Resources Utilization (MRU), Japan Agency for Marine-Earth Science and Technology (JAMSTEC), Yokosuka 237-0061, Japan
[e] Research Institute for Global Change (RIGC), Japan Agency for Marine-Earth Science and Technology (JAMSTEC), Yokosuka 237-0061, Japan
[f] Geological Survey of Japan, National Institute of Advanced Industrial Science and Technology (AIST), Central 7, 1-1-1 Higashi, Tsukuba, Ibaraki 305-8567, Japan
[g] Department of Materials, Environmental Sciences and Urban Planning, Polytechnic University of Marche, Via Brecce Bianche, 60131 Ancona, Italy
[h] Institute of Marine Sciences, National Research Council (ISMAR-CNR), Arsenale, Tesa 104, Castello 2737/F, 30122 Venice, Italy
[i] Stazione Zoologica Anton Dohrn, Villa Comunale, 80121 Naples, Italy
[j] Department of Life and Environmental Sciences, Polytechnic University of Marche, Via Brecce Bianche, 60131 Ancona, Italy
[k] Research Center for Bioscience and Nanoscience (CeBN), Japan Agency for Marine-Earth Science and Technology (JAMSTEC), Yokosuka 237-0061, Japan
[l] Hellenic Center for Marine Research (HCMR), 710 03 Heraklion, Crete, Greece
[m] Department of Biology & CESAM, University of Aveiro, Campus de Santiago, Aveiro 3810-193, Portugal

ARTICLE INFO

Keywords:
Abyssal plains
Particulate organic carbon
Benthic organisms
Virus
Food-webs
Vertical distribution
Western Pacific Ocean

ABSTRACT

The abyssal plain covers more than half the Earth's surface. The main food source to abyssal ecosystems is phytodetritus, which originates from phytoplankton in the surface ocean, and thus its variability to the seafloor is a major driver of abyssal ecosystem biomass and functioning. In this study, we conducted a comparative survey on organic matter (OM) quality and quantity in abyssal plain sediments and examined the distributions of megafauna, macrofauna, meiofauna, prokaryotes, and viruses in eutrophic (39°N), oligotrophic (1°N), and ultra-oligotrophic (12°N) areas of the western Pacific. We also analyzed stable carbon and nitrogen isotopic compositions of organisms at 39°N and 1°N to assess differences in benthic abyssal food-web structures with contrasting trophic states. Sediments collected at 39°N presented highest concentrations of total organic carbon (TOC) and labile OM, and high diffusive oxygen uptake rates. By contrast, the lowest values were found at 12°N. Vertical distributions of sediment macrofauna, meiofauna, and prokaryotes matched with labile OM profiles. There were prominent differences in abundances of macro- and megafauna among stations with different OM fluxes, whereas the abundance of meiofauna and prokaryotes showed smaller differences among stations. Such differences could be explained by higher turnover rates of smaller organisms. Food-web structures of abyssal plains are likely influenced by both the type and size of primary producers in surface ocean. Our results underscore the crucial importance of OM fluxes and their compositions to the abundances and vertical profiles of labile OM and benthic biota in abyssal ecosystems.

1. Introduction

The abyssal plain covers more than half of Earth's surface and plays important roles in ecosystem functioning and biogeochemical cycles and as a major reservoir of biodiversity. Food supply to abyssal plain ecosystems is composed of particulate organic matter (POM) derived from

* Corresponding author.
E-mail address: nomakih@jamstec.go.jp (H. Nomaki).

https://doi.org/10.1016/j.pocean.2021.102591
Received 26 November 2020; Received in revised form 18 April 2021; Accepted 20 April 2021
Available online 3 May 2021

the surface ocean. Phytoplankton produce organic matter (OM) by fixing inorganic carbon originating from atmospheric CO_2. A small fraction of the OM is transported out of the photic zone as POM (Buesseler et al., 2007) into the underlying deep waters in the form relatively large aggregate of phytodetritus and faecal pellets sinking at a rate of > 100 m d^{-1}. During this process, settling POM is partly degraded or respired by heterotrophs on its way to the seafloor (Turley et al., 1995). The quantity and quality of this POM transport to the abyssal plain can be highly variable, particularly with fluctuations in phytoplankton community structure during spring blooms occurring on a timescale of weeks (Billett et al., 1983; Smith et al., 1997; Beaulieu, 2002). This variability has been hypothesized to alter patterns of faunal abundance, diversity, and ecosystem functioning on the abyssal plain (Ruhl and Smith, 2004; Smith et al., 2009, 2013; Billett et al., 2010; Amaro et al., 2019).

The importance of particulate organic carbon (POC) fluxes to abyssal ecosystems has been demonstrated through continuous monitoring of abyssal stations over several decades (Smith et al., 2009, 2020). For example, long-term monitoring in the two temperate areas of the North Atlantic (Porcupine Abyssal Plain: Billett et al., 2001) and eastern North Pacific (Station M: Laureman et al., 1996; Ruhl and Smith, 2004; Smith et al., 2006) has been used to identify seasonal variations in POC flux and has helped reveal the impacts of these variations on benthic organisms (from prokaryotes to megafauna) and biogeochemical cycles. Recent studies have further indicated that decadal-scale shifts in primary production associated with the El Niño–Southern Oscillation (ENSO) can produce long-term changes in deep-sea benthic communities (Billett et al., 2001, 2010; Ruhl and Smith, 2004; Ruhl, 2007; Smith et al., 2008, 2009). This tight coupling between surface and abyssal plain ecosystems suggests that anthropogenic impacts (e.g., warming temperatures, acidification, and pollution) could have strong effects on seafloor biota (Giordani et al., 2002; Danovaro et al., 2017). This emphasizes the necessity of monitoring abyssal ecosystems and their functioning in order to understand the effects of natural and human-derived changes in the deep sea (Paull et al., 2002; Smith et al., 2009, 2020; Ramirez-Llodra et al., 2011; Schlining et al., 2013; Barry et al., 2014; Chiba et al., 2018; Danovaro et al., 2020).

However, due to the remoteness of the abyssal seafloor, studies of biodiversity and ecosystem functioning in the abyssal depths have been confined to limited areas. This is particularly true for oligotrophic and ultra-oligotrophic regions, which have received even less attention. The effects of POC fluxes on sedimentation processes, microbial biomass, and macro- and megafaunal abundances were investigated along latitudinal POC flux gradients in the eastern equatorial Pacific from 12°S to 9°N (Smith et al., 1997). The study identified significant correlations between POC fluxes and both faunal abundance and prokaryote biomass, thereby confirming the importance of POC fluxes in abyssal ecosystems. In the oligotrophic western North Pacific abyssal plain ecosystem, meiofaunal abundances were found to be correlated with food availability and meiofauna was largely confined to the top 1 or 2 cm of sediment (Shirayama, 1984a, 1984b). However, no studies to date have characterized the effects of POC fluxes to abyssal plains under multiple ecological provinces of the ocean across a range of surface productivity (Sonnewald et al., 2020). Ecological provinces are characterized by the differences in plankton community structures and associated nutrient fluxes. Diatoms, which are generally large-bodied, are dominant at higher latitudes (i.e., under *meso*-eutrophic conditions), whereas picoplankton and small dinoflagellates predominate at lower latitudes (i.e., more oligotrophic conditions). As both the species and size of primary producers can impact on POC fluxes through changes in transfer efficiency (Buesseler et al., 2007) and are therefore expected to influence deep-sea benthos, it is essential to investigate the nature of abyssal ecosystems and relevant biogeochemical cycles in relation to overlying surface productivities across wide latitudinal ranges.

In this study, we investigated how biotic compartments of different size classes (viruses, prokaryotes, and meio-, macro-, and megafauna) respond to environmental factors in three abyssal benthic ecosystems in the western Pacific characterized by different levels of surface productivity. We chose three sampling stations (at 39°N, 1°N, and 12°N) with differing surface primary productivity (corresponding to eutrophic, oligotrophic, and ultra-oligotrophic conditions, respectively). Additionally, the three stations provide contrasts in biomass and compositions of surface primary producers and belong to three different ecological provinces (Sonnewald et al., 2020). We undertook a comprehensive assessment of sediment geochemistry at each station by collecting porewater dissolved oxygen and nutrient concentration profiles, among other measurements, and we investigated the quantity and quality of OM constituents such as lipids, proteins, carbohydrates, and pheopigments to understand how these parameters relate to surface primary production. We also tested correlation among the abundances and vertical distributions of different organism size classes and geochemical parameters. Finally, we used natural stable-isotope signatures to assess the effect of different primary production regimes at two of the three western Pacific stations.

2. Material and methods

2.1. Study area

Four sampling cruises were conducted at three abyssal stations in the Northwest Pacific Ocean in September–November 2013 (JAMSTEC cruises YK13-09 and YK13-12) and May–July 2014 (YK14-06 and YK14-12) aboard the R/V *Yokosuka*. Station 39°N (39°00.0′N 146°00.1′E, water depth 5260 m) is located on the seaward side of the Japan Trench, Station 1°N (01°15.0′N 163°14.8′E, water depth 4277 m) is located northeast of the Ontong Java Plateau, and Station 12°N (11°59.9′N 153°59.9′E, water depth 5920 m) is located on the western side of the Mariana Trench (Fig. 1). We selected the abyssal plain sites without depressions or hills to minimize any topographic effects on faunal composition and abundance (Durden et al., 2015; Stefanoudis et al., 2016). POC fluxes to the seafloor are 1086 mgC m^{-2} yr^{-1}, 485 mgC m^{-2} y^{-1}, and 191 mgC m^{-2} y^{-1} at stations 39°N, 1°N, and 12°N, respectively, based on the equation described by Lutz et al. (2007). Sediments at Station 39°N consisted of diatomaceous ooze, and those at Station 1°N consisted of red clay and planktonic foraminiferal tests. Surface sediments at Station 12°N consisted of red clay. During a submersible dive at Station 39°N on 4 May 2014, we observed patchy distribution of several-centimeter-sized orange-brown detrital aggregates on the seafloor (Amaro et al., 2019). However, these aggregates were not present on 1 July. No detrital aggregates were observed at stations 1°N and 12°N.

2.2. Organisms and sediment sampling

Megafaunal abundances were estimated from video surveys conducted during *Shinkai 6500* dives at each station. Details of the video surveys and megafaunal abundance estimates were previously described in Amaro et al. (2019). Megafauna (more specifically, holothurians) were also collected with a suction sampler attached to the *Shinkai 6500* with six exchangeable rotating containers equipped with a 30-μm mesh at the outlet. Once the submersible was back on board, the specimens were placed immediately in a temperature-controlled laboratory (4 °C).

Surface sediments and benthic organisms were collected during the dives of manned submersible *Shinkai 6500*. Surface sediments were collected with a push corer with an inner diameter of 82 mm and core tube lengths of either 320 or 500 mm. Upon recovery, sediment cores were stored in a cold room (4 °C) and then processed as described below.

2.3. Oxygen concentrations in sediments

Dissolved oxygen (DO) concentrations in the sediment cores were measured onboard immediately after core recovery using a planar

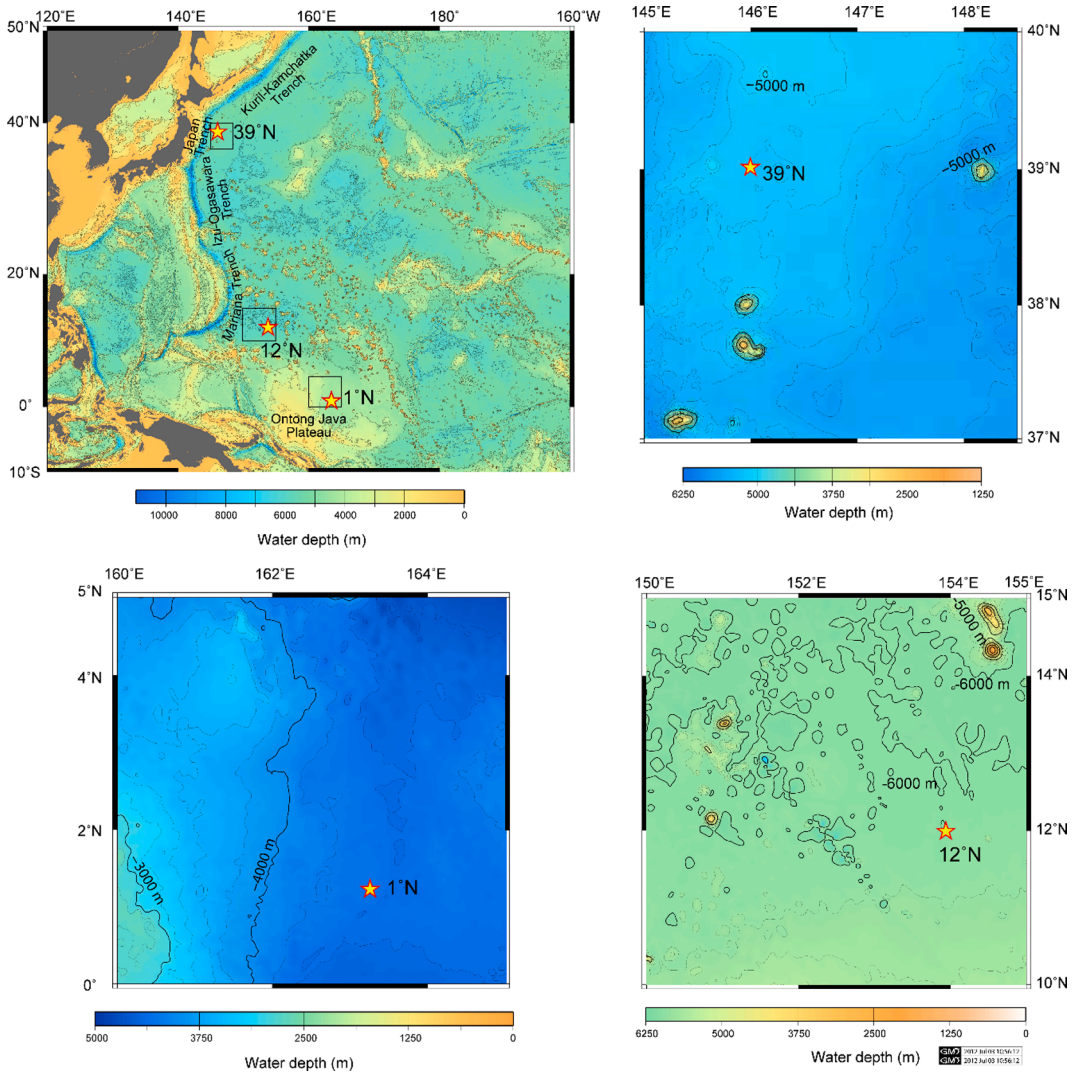

Fig. 1. Sampling stations on the western Pacific abyssal plain (upper left). Station 39°N: 39°00.0′N, 146°00.1′E, water depth = 5260 m (upper right). Station 12°N: 11°59.9′N, 153°59.9′E, water depth = 5920 m (lower right). Station 1°N: 1°15.0′N, 163°14.8′E, water depth = 4277 m (lower left).

optode oxygen sensor Fibox 3 (PreSens, Regensburg, Germany). Sensor spots were attached to the inside of the transparent polycarbonate core liner tube at 2-cm depth intervals, and oxygen concentrations were measured from the outside through the tube wall (Hiraoka et al., 2020). The optode sensor was calibrated against air-saturated and oxygen-free seawater before measurements. At Station 39°N, DO profiles across the sediment–water interface were also obtained by using an oxygen microelectrode with a tip diameter of 100 μm (Unisense, Aarhus, Denmark). DO was measured from approximately 5 to 10 mm above the sediment surface down to 30–40 mm sediment depth in 500-μm steps by using an automatic profiler controlled by Sensor Trace Pro software (Unisense).

Diffusive oxygen uptake (DOU) across the sediment–water interface was calculated from the concentration gradient of the optode data by using Fick's first law of diffusion, the whole-sediment diffusion coefficient reported in Ullman and Aller (1982), and the measured porosity at each station (K Seike, unpublished results). As the vertical resolution of DO profiles are low, DOU rates calculated in this study may be underestimated, thus we mainly use these values for the comparisons among stations.

2.4. Biochemical composition of sedimentary OM and extracellular enzymatic activities

The concentrations of proteins, carbohydrates, and lipids in the collected sediments were measured by using photometric protocols, as previously reported for stations 39°N and 1°N (Amaro et al., 2019).

Concentrations of chlorophyll *a* and its degradation products (i.e., pheopigments) were used as an index of fresh phytoplankton-derived OM in sediment samples obtained at each station and were measured using the protocol described in Naeher et al. (2016). In brief, frozen sediment samples were freeze-dried and ground into powder, and 1–300 g of dry sediments were extracted three times with acetone by ultrasonification for 15 min in an ice bath, followed each time by centrifuging at 777*g* for 5 min. The extracts were further purified and subdivided in several steps using high-performance liquid chromatography (HPLC) (Agilent 1100 series: Agilent Technologies, Santa Clara, USA) with relevant columns and methods as reported previously (Naeher et al 2016). Concentrations of each pheopigment were determined by using HPLC.

Extracellular enzymatic activity (aminopeptidase and β-glucosidase) was measured by means of time course experiments at *in situ* temperature under dark conditions (Danovaro, 2010). Aminopeptidase and β-glucosidase activities were inferred from cleavage rates of the artificial

fluorogenic substrates L-leucine-4-methylcoumarinyl-7-amide and 4-methylumbelliferyl-b-D-glucopyranoside (Sigma Chemicals, Milan, Italy), respectively, under saturating substrate concentrations. Enzymatic activities were measured in three replicates, and data were normalized to sediment dry weight after desiccation (48 h at 60 °C).

2.5. Abundance of prokaryotic cells and viruses

At stations 39°N and 1°N, sediment samples were sliced into the following depth layers: 0–1 cm, 1–3 cm, 3–5 cm, and 5–10 cm. At Station 12°N, only the 0–1 cm depth layer was sampled. Prokaryotic and viral abundances were determined by epifluorescence microscopy after extraction of cells and viruses from the sediment using pyrophosphate (final concentration, 5 mM), sonication, and staining with SYBR Green I as described in Danovaro (2010). Both prokaryotic and viral abundances were analyzed in three replicates, and data were normalized to sediment dry weight after desiccation (48 h at 60 °C).

2.6. Meiofauna, macrofauna, and megafauna analysis

Sediment cores were sliced horizontally into the following depth layers: 0–1 cm, 1–2 cm, 2–3 cm, and 3–5 cm. At Station 39°N, sediment cores were further sliced into 5–7 cm, 7–10 cm, and 10–15 cm. Sliced sediment samples were fixed immediately in 10% buffered formalin to be a final concentration of 4% diluted in seawater and mixed with Rose-Bengal dye (0.05 g L^{-1}). In the laboratory, each sediment sample was carefully washed with pre-filtered artificial seawater through 250-μm and 32-μm mesh sieves.

Sediments remaining on the 32-μm mesh sieve were re-suspended and centrifuged three times with colloidal silica (Ludox HS40; Sigma-Aldrich, St. Louis, Missouri, USA) according to the method described in Danovaro (2010). The supernatant was transferred to a Petri dish with a 5-mm grid on the bottom, and Rose-Bengal stained organisms (i.e., meiofauna) were sorted to higher taxonomic levels and counted under a binocular stereoscopic microscope according to the methods described in Giere (2009). Note that we used a 250-μm mesh for the upper limit of meiofaunal analyses, which was smaller than the typical size limit of 500-μm (Giere 2009).

We also isolated any soft-walled foraminifera contained in the supernatant. However, some foraminifera with calcareous tests, as well as agglutinated taxa attaching large mineral particles (e.g., *Reophax*), were likely overlooked in this study. In our data set, most komokiaceans (either complete or fragmented forms) and large-sized species that are abundant at abyssal plains (e.g. Goineau and Gooday 2017) were not included because we did not pick foraminifera from the sediment residues retained on the 250 μm mesh. No sample splitting was performed before the isolation of meiofauna; thus, all meiofauna in the supernatant of the entire sample were counted. Meiofaunal abundance was calculated as the number of individuals per 10 cm^3 for each sediment depth (Nomaki et al., 2016).

Metazoans retained on the 250-μm sieves, which we refer as macrofauna, were sorted into major taxa and identified to the species level whenever possible. Species abundance was determined for each sediment layer in each replicate core. Macrofauna abundances were calculated as the number of individuals per m^2 of sampling area (i.e., ind. m^{-2}). Each specimen was stored for analysis of C and N isotopic compositions. Macrofauna were examined only at stations 39°N and 1°N, not at Station 12°N.

Among the recovered holothurians, only intact specimens were selected for isotopic composition analysis (Amaro et al., 2019). Each specimen was dissected in a sterilized Petri dish using sterilized spatulas. After dissection, body wall samples were stored in clean, aluminum foil-wrapped, pre-weighed Petri dishes at –80 °C. In the laboratory, samples were freeze-dried and then frozen in liquid nitrogen and ground to a coarse powder with a pestle and motor, and finally stored at –20 °C prior to analysis.

2.7. C and N contents and isotopic compositions

Approximately 1 ml of each subdivided sediment was used to examine total organic carbon (TOC), total nitrogen (TN) and their isotopic compositions ($\delta^{13}C$ and $\delta^{15}N$) (for details, see Amaro et al., 2019; Nomaki et al., 2019). The samples were freeze-dried, powdered, and weighed into pre-cleaned silver capsules (Ogawa et al., 2010), and then they were decalcified with 2 M HCl, followed by drying on a hot plate at 60 °C. Dried silver capsules containing decalcified samples were sealed into pre-cleaned tin capsules prior to isotopic analysis.

Macrofauna and meiofauna samples were placed directly into pre-cleaned tin capsules and dried at 60 °C to remove water and determine dry weight. After weighing, the samples were decalcified with 0.1 M HCl and completely dried again, and the capsules were sealed using pre-cleaned forceps.

C and N isotopic compositions along with the TOC and TN content of decalcified samples were determined by using three different isotope ratio mass spectrometer (IRMS) coupled to an elemental analyzer (EA) systems according to their sample types. In brief, sediment samples were analyzed by Flash EA1112-ConFloIV DELTA V Advantage System (Thermo Fisher Scientific, USA) at SI Science Co. ltd, Japan, macrofauna samples were analyzed by Flash EA1112- ConFloIV DELTA plus Advantage System (Thermo Fisher Scientific, USA) at JAMSTEC, and meiofauna were analyzed by a modified system of Flash EA1112-ConFloIII Delta plus XP (Thermo Finnigan, Germany, Ogawa et al., 2010). The isotope ratios were expressed in delta-notation as $\delta X = [(R_{sample}/R_{standard}) - 1] \times 1000$, where X is ^{13}C or ^{15}N and R is the ratio ^{13}C:^{12}C or ^{15}N:^{14}N. Analytical errors for $\delta^{13}C$ and $\delta^{15}N$ standards were both within ± 0.18‰ (SD, 1σ) for all three EA/IRMS.

Meiofaunal biomass (TOC weight) was determined from the C content of samples measured with EA/IRMS. Macrofaunal biomass was also determined by using EA/IRMS; however, for large biomass specimens (generally over 250 μgC), a part of the specimen (typically muscle tissue) was sub-sampled for EA/IRMS, and dry weights of both the EA/IRMS subsample and the remaining specimen were measured. The TOC weight % of the remainder was assumed to be the same as the TOC weight % of the subsample, and the TOC content of the specimen was calculated as the TOC weight % multiplied by the total dry weight.

2.8. Statistical analysis

Differences in analyzed parameters were tested with ANOVA (analysis of variance) for comparisons among three stations and student's *t*-tests for comparisons between two stations (station 39°N and 1°N, for macrofaunal analysis). Although ANOVA and *t*-test are robust against the assumptions on normality and equivariance (Zar, 2010), we performed Shapiro-Wilk tests for normality and Bartlett's tests or *F* tests to test whether samples have equal variance before performing ANOVA and *t*-tests. The results showed that the null-hypnoses were not rejected ($p > 0.05$) for almost all data, while a few cases the null-hypnoses were rejected; 3 among 54 tests were deviate from normality and 1 among 18 tests were deviate from equivariance, (Supplementary Table 1). When significant differences were detected among three stations by ANOVA, post-hoc Tukey's honestly significant difference (HSD) tests were performed to identify which combination of stations were significantly different. Correlations of organism (prokaryotes, nematodes, copepods, foraminifera, and total macrofauna) and virus abundances with environmental parameters (DO, TOC, TN, water content, nutrient concentration, pheophytin-*a*, and total pheopigment) were tested with simple correlation analysis. For prokaryotes and viruses, correlation analysis was performed for sediment depths of up to 10 cm, and for meiofauna and macrofauna, up to 5 cm. All parameters were log-transformed prior to analysis. All statistical analyses were conducted with R studio (RStudio Team, 2016).

3. Results

3.1. Sediment geochemistry and extracellular enzymatic activities

TOC and TN concentrations decreased with sediment depth at all stations, but they showed substantial differences among stations (Fig. 2A, Table 1). The lowest TOC concentrations were observed at Station 12°N, where they decreased from 0.45% in the uppermost layer (0–1 cm) to 0.2% at depths greater than 30 cm. TOC concentrations in the 0–1 cm sediment layer were higher at stations 1°N and 39°N and decreased more sharply with depth at Station 1°N than at Station 39°N (Fig. 2A).

Carbon isotopic compositions ($\delta^{13}C$) of TOC at the eutrophic Station 39°N differed substantially from those at stations 1°N and 12°N (Table 1). At Station 39°N, mean $\delta^{13}C$ value was –20.8‰ and stayed almost constant with depth, ranging from –21.0 to –20.7‰. At stations 1°N and 12°N, $\delta^{13}C$ values in the 0–1 cm sediment depth layer were both –19.5‰ and varied slightly with depth, ranging from –19.7 to –18.9‰ and from −20.8 to –19.3‰, respectively.

Nitrogen isotopic compositions ($\delta^{15}N$) also differed substantially among stations. In the 0–1 cm depth layer, $\delta^{15}N$ values of TN were 7.0‰, 9.8‰, and 12.0‰ at stations 39°N, 12°N, and 1°N, respectively (Table 1). $\delta^{15}N$ values remained almost constant with depth at all three stations.

DO concentration profiles in the sediment column varied among the three stations, but concentrations in the bottom water were similar (ranging from 170 to 190 μM O_2) (Fig. 2B). At Station 39°N, DO concentrations decreased sharply in the first few centimeters of sediment, reaching almost 0 μM at a depth of 7 cm based on the optode measurements and at a depth of approximately 2–3 cm based on the microelectrode (Supplementary Fig. 1). At Station 1°N, DO concentrations in the first 5 cm of sediment decreased less sharply than at Station 39°N and decreased especially gradually below a depth of 10 cm, reaching a concentration of 80 μM at a depth of 30 cm. At Station 12°N, oxygen concentrations decreased gradually throughout the entire depth profile and reached a concentration of 140 μM at a sediment depth of 30 cm. Calculated DOU rates were 243, 46.6, and 18.9 μM O_2 m^{-2} d^{-1} at stations 39°N, 1°N, and 12°N, respectively.

Concentrations of chlorophyll *a* and its degradation products varied considerably among the stations (Fig. 3). Pheophytin *a* (Phe *a*) concentrations at Station 39°N ranged between 280 and 500 ng g^{-1} dry sediment throughout the sediment column, and those at stations 1°N and 12°N ranged from 0.2 to 17 ng g^{-1} and from 0.1 to 1.0 ng g^{-1} dry sediment, respectively. Pyropheophytin *a* (PPhe *a*) was the second most abundant pheopigment, ranging from 200 to 450 ng g^{-1} dry sediment at Station 39°N and from 0 to 8.2 ng g^{-1} dry sediment at Station 1°N, followed by steryl chlorin esters (SCEs) as the third most abundant pheopigment. Chlorophyll *a*, which is indicative of the most intact (i.e., fresh) pheopigment, was only detected in the 10–15 cm sediment depth layer at Station 39°N (Fig. 3). It is noteworthy that pheopigment concentrations decreased with increasing sediment depth at Station 1°N, but not at Station 39°N. Only one pheopigment (Phe *a*) was identified at Station 12°N throughout the entire examined depth.

Concentrations of carbohydrates, proteins, and lipids in the uppermost sediment layer (0–1 cm) were highest at Station 39°N.

Table 1
Total organic carbon (TOC) concentrations, total nitrogen (TN) concentrations, and carbon and nitrogen isotopic compositions ($\delta^{13}C$ and $\delta^{15}N$, respectively) of sediments collected from three abyssal stations in the western Pacific.

Site	Sediment depth (cm)	TOC (wt %)	TN (wt %)	$\delta^{13}C$ (‰)	$\delta^{15}N$ (‰)
39°N	0–1	1.40	0.204	−20.8	7.0
	1–2	1.42	0.207	−20.8	6.9
	2–3	1.31	0.193	−20.7	7.3
	3–5	1.25	0.182	−20.7	7.2
	5–7	1.34	0.187	−20.8	6.7
	7–10	1.24	0.178	−20.8	6.4
	10–15	1.12	0.158	−20.8	6.6
	15–20	1.16	0.161	−21.0	6.6
1°N	0–1	1.33	0.224	−19.5	12.0
	1–2	1.30	0.215	−19.7	12.1
	2–3	1.25	0.207	−19.7	12.3
	3–4	1.01	0.178	−19.5	12.1
	4–5	1.04	0.169	−19.4	11.7
	5–6	1.13	0.192	−19.2	12.4
	6–8	1.10	0.180	−19.1	12.9
	8–10	0.94	0.166	−19.5	12.6
	10–15	0.83	0.147	−19.5	12.3
	15–20	0.86	0.142	−19.0	11.7
	20–25	0.76	0.140	−18.9	11.5
12°N	0–1	0.46	0.115	−19.5	9.8
	1–4	0.38	0.095	−19.5	9.7
	4–7	0.43	0.104	−19.6	10.0
	7–10	0.33	0.092	−19.3	9.6
	10–15	0.30	0.091	−19.8	9.5
	15–20	0.25	0.083	−19.9	9.0
	20–25	0.29	0.092	−20.2	9.9
	25–30	0.26	0.084	−20.6	9.3
	30–35	0.19	0.072	−20.6	9.1
	35–40	0.20	0.073	−20.8	9.1

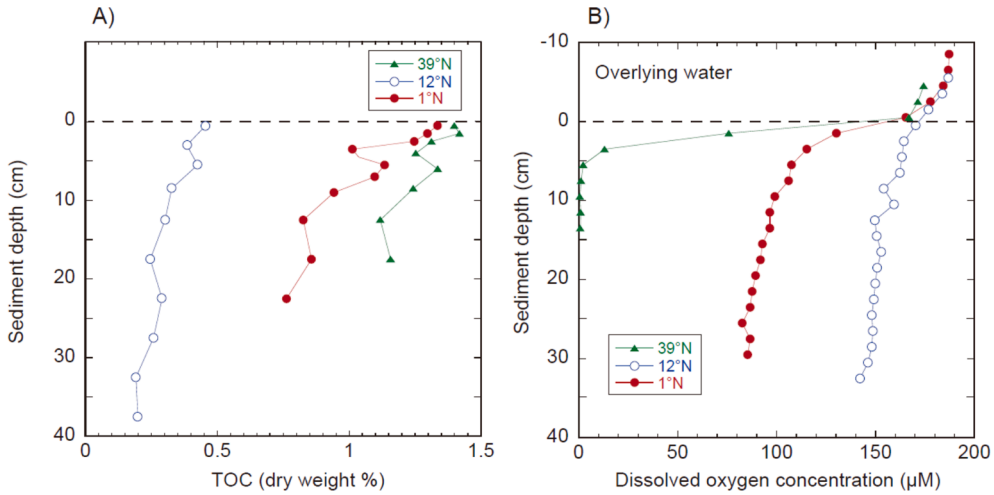

Fig. 2. (A) Total organic carbon (TOC) contents and (B) dissolved oxygen (DO) concentrations of natural background sediments collected from the three abyssal stations. DO profiles presented here were measured with an optode-type oxygen sensor spot. DO profiles measured by using a glass-microelectrode at Station 39°N are not shown.

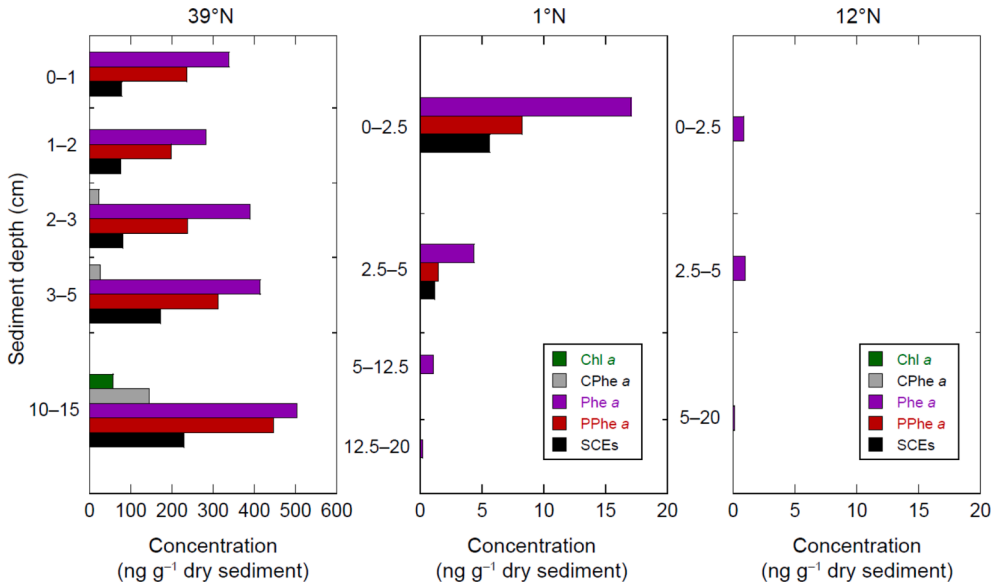

Fig. 3. Concentrations of chlorophyll *a* and its degradation products at different sediment depths at the three abyssal stations. Chl *a*, chlorophyll *a*; CPhe *a*, 13^2,17^3-cyclopheophorbide-*a*-enol; Phe *a*, pheophytin *a*; PPhe *a*, pyropheophytin *a*; SCEs, steryl chlorin esters. Note that we examined different sediment depth intervals at each station.

Carbohydrate concentrations were 1.9–5.6-fold higher than at the oligotrophic stations 1°N and 12°N. Similarly, protein concentrations were 2.8–7.4-fold higher and lipid concentrations were 1.7–4.3-fold higher (Supplementary Fig. 2, Table 2).

Aminopeptidase activity at Station 39°N was 1.9–4.8-fold higher than at Station 1°N, and 4.5–12.9-fold higher than at Station 12°N (Supplementary Fig. 3; Table 2). Conversely, the highest β-glucosidase activity was found at Station 12°N, and it was on average 2.2 ± 0.6-fold higher than at stations 39°N and 1°N (Supplementary Fig. 3; Table 2).

3.2. Prokaryotic and viral abundances

Prokaryotic abundances in the 0–1 cm sediment layer did not differ significantly among the three stations (Fig. 4, Table 2). In contrast, prokaryotic abundances below 1 cm were higher at Station 39°N than at Station 1°N (Fig. 4). Prokaryotic abundances at Station 39°N ranged from 4.7 to 5.6 × 10^7 cells g^{-1} throughout the sediment column, and at Station 1°N, they decreased with sediment depth from 3.6 ± 0.7 × 10^7 cells g^{-1} (in the 0–1 cm depth layer) to 1.4 ± 0.5 × 10^7 cells g^{-1} (in the 5–10 cm depth layer). Note that prokaryotic and viral abundances were not measured at Station 12°N below a sediment depth of 1 cm.

Viral abundance in the 0–1 cm sediment depth layer was almost 10-fold higher at Station 39°N (6.4 ± 0.29 × 10^8 viruses g^{-1}) than at stations 1°N (6.8 ± 0.8 × 10^7 viruses g^{-1}) and 12°N (5.7 ± 0.7 × 10^7 viruses g^{-1}) (Fig. 4). Viral abundance in the 1–2 cm sediment layer was approximately 50% of those in the 0–1 cm layer at stations 39°N and 1°N. Viruses were more abundant at Station 39°N than at Station 1°N throughout the sediment column (Fig. 4).

The virus-to-prokaryote ratio (VPR) in the 0–1 cm sediment layer at Station 39°N (15.6 ± 5.3) was approximately 8 times higher than at stations 1°N (1.9 ± 0.6) and 12°N (1.8 ± 0.4) (Fig. 4). The VPR at Station 39°N was higher than at Station 1°N throughout the sediment column.

Table 2
ANOVA results for prokaryotic cell numbers, viral abundances, and organic matter concentrations measured at three abyssal sites. Post-hoc Tukey's HSD tests were conducted when ANOVA detected significant differences among sites.

	F-value	*p*-value	39°N vs. 1°N	39°N vs. 12°N	1°N vs. 12°N
Viral abundance (0–1 cm)	480.5	<0.001	<0.001	<0.001	n.s.
Prokaryotic cell numbers (0–1 cm)	0.889	n.s.			
Aminopeptidase activity	65.1	<0.001	<0.01	<0.001	<0.01
β-glucosidase activity	15.2	<0.01	n.s.	<0.01	<0.05
Carbohydrates	171.7	<0.001	<0.001	<0.001	<0.001
Proteins	120.7	<0.001	<0.001	<0.001	<0.01
Lipids	12.2	<0.01	<0.01	<0.05	n.s.
Biopolymeric C	45.3	<0.001	<0.01	<0.001	<0.05

n.s.: Not significant.

3.3. Meiofaunal abundance and assemblage composition

Total meiofaunal abundance was highest at Station 39°N and lowest at Station 12°N (Fig. 5). Although there were no statistically significant differences among the three stations in the 0–1 cm sediment layer (Table 3, ANOVA, $F = 3.27$, $p > 0.05$), significant differences were detected in total abundance of 0–5 cm sediment such that Station 39°N had the highest abundance and Station 12°N the lowest (Table 3, ANOVA, $F = 37.84$, $p < 0.001$). Nematode and copepod abundances also followed the same trend (Table 3, Fig. 5). In contrast, the abundance of soft-walled foraminifera mainly consisted of monothalamids did not differ significantly among stations in the 0–1 cm sediment layer or in the 0–5 cm layer.

Nematodes dominated meiofaunal abundances at all three stations. They accounted for 85.1% of the total meiofaunal community at Station 39°N, followed by foraminifera (5.1%) and copepods (4.6%) (Fig. 5). At Station 1°N, nematodes accounted for 74.0% of total meiofaunal abundance, followed by foraminifera (17.7%) and copepods (3.3%). At Station 12°N, nematodes accounted for 71.5% of total meiofaunal abundance, followed by foraminifera (20.7%) and copepods (2.5%). Nematodes were also dominant in terms of biomass, accounting for 74.3% of total meiofaunal biomass at Station 39°N and 66.2% at Station 1°N (Table 4). Copepods accounted for 11.9% and 8.8% of meiofaunal biomass at stations 39°N and 1°N, respectively, and foraminifera accounted for 8.0% and 12.6% at stations 39°N and 1°N, respectively. At Station 12°N, both nematodes (38.1%) and foraminifera (34.7%) accounted for a large percentage of total meiofaunal biomass, followed by meiofaunal polychaetes (19.3%) and copepods (7.4%).

At Station 39°N, nematodes and foraminifera were most abundant in

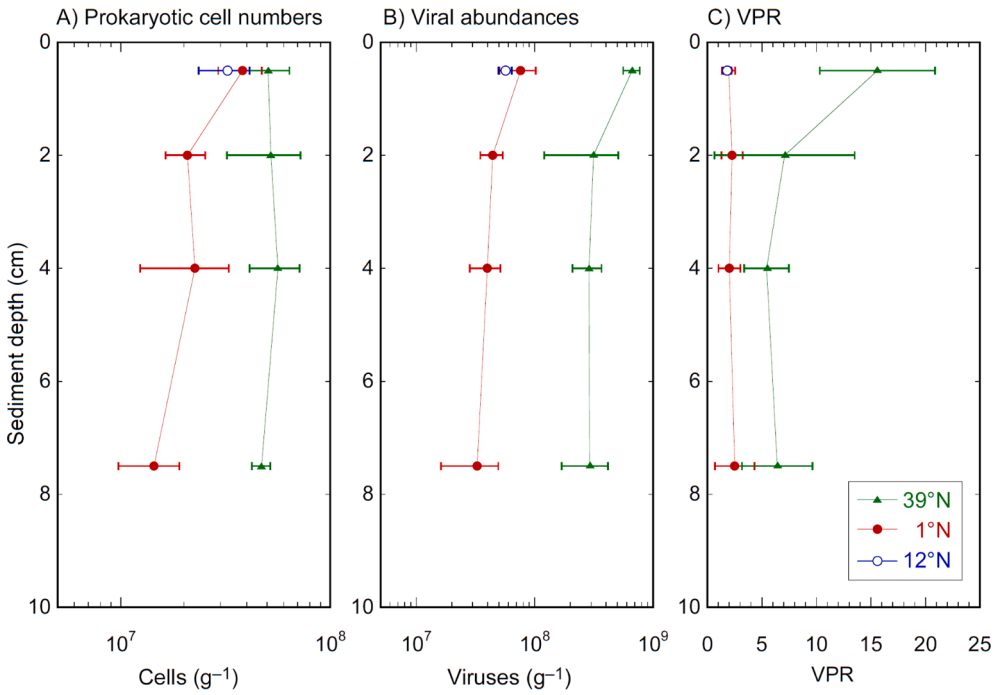

Fig. 4. Vertical profiles of (A) prokaryotic cell numbers, (B) viral abundances, and (C) virus-to-prokaryote ratio (VPR) in sediments at stations 39°N and 1°N. Error bars indicate standard deviations calculated from three replicate samples.

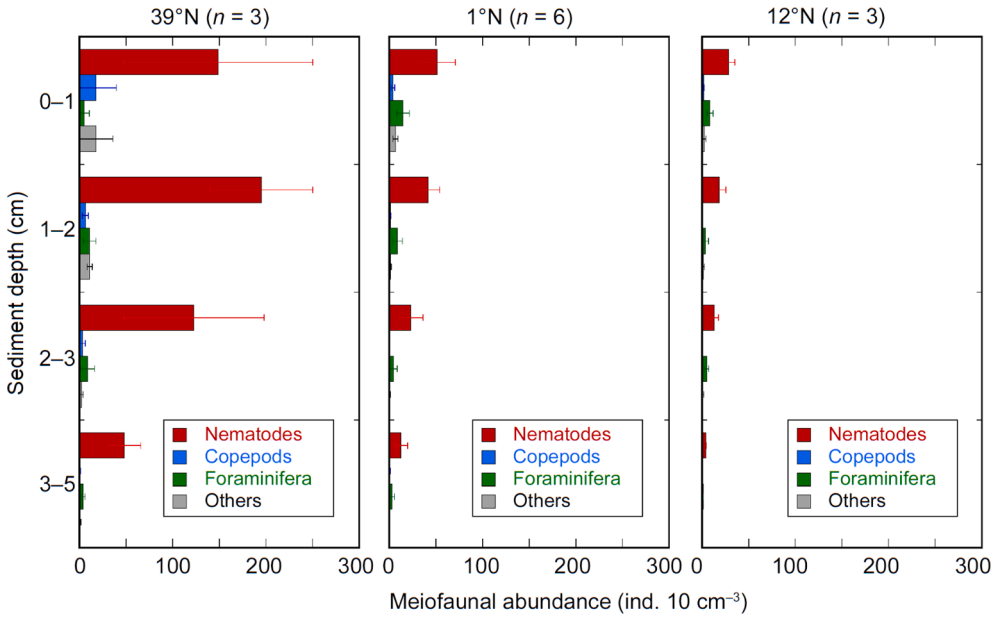

Fig. 5. Meiofaunal abundance (samples between 32-μm to 250-μm mesh sieves) at three sampling stations on the western Pacific abyssal plain. Abundances are reported as individuals per 10 cm^3. Error bars indicate standard deviations calculated from replicate cores. Note that we did not include hard-shelled foraminifera in this study. As a result, the foraminifera analysed comprised mainly monothalamids.

the 1–2 cm sediment layer, and copepods were most abundant in the 0–1 cm layer (Fig. 5). At stations 1°N and 12°N, nematodes, copepods, and foraminifera were most abundant in the 0–1 cm sediment layer, and their abundances decreased gradually with depth in sediments.

3.4. Macro- and megafaunal abundance and assemblage composition

Macrofaunal abundance in the 0–1 cm sediment layer was approximately 3-fold higher at Station 39°N (290 ± 48 ind. m^{-2}) than at Station 1°N (93 ± 54 ind. m^{-2}) ($t = 4.90, p < 0.01$) (Fig. 6). The total abundance of the four shallowest layers (i.e., 0–5 cm) was 7-fold higher at Station 39°N than at Station 1°N ($t = -9.13$, $p < 0.001$).

Macrofaunal abundance at Station 39°N was largely dominated by nematodes (71.2%), followed by Arthropoda (12.8%), Annelida (5.4%), and Mollusca (5.2%) (Fig. 6A). At Station 1°N, macrofaunal abundance was dominated by Arthropoda (38.1%), followed by Nematoda (35.7%), Annelida (9.5%), and Mollusca (4.8%). Macrofaunal biomass, in terms of C content, was 12-fold higher at Station 39°N (111.5 mgC m^{-2}) than at Station 1°N (9.1 mgC m^{-2}). Macrofaunal biomass at Station 39°N was dominated by Annelida (49.1%), followed by Mollusca (20.8%),

Table 3
ANOVA results for meiofaunal abundances measured at three abyssal sites. Post-hoc Tukey's HSD tests were conducted when ANOVA detected significant differences among sites.

	F-value	*p*-value	39°N vs. 1°N	39°N vs. 12°N	1°N vs. 12°N
0–1 cm					
Total meiofauna	3.27	n.s.			
Nematodes	4.23	n.s.			
Copepods	2.13	n.s.			
Foraminifera	3.12	n.s.			
0–5 cm					
Total meiofauna	37.84	<0.001	<0.001	<0.001	<0.05
Nematodes	49.84	<0.001	<0.001	<0.001	<0.05
Copepods	22.44	<0.001	<0.01	<0.001	<0.05
Foraminifera	1.66	n.s.			

n.s.: Not significant.

Table 4
Meiofaunal biomass (samples between 32-μm to 250-μm mesh sieves) at three abyssal stations in the western Pacific. Note that we did not include hard-shelled foraminifera in this study. As a result, the foraminifera analysed comprised mainly monothalamids.

	39°N		1°N		12°N	
	mgC m^{-2}	% Biomass	mgC m^{-2}	% Biomass	mgC m^{-2}	% Biomass
Nematodes	9.19	74.3	5.26	66.2	1.33	38.1
Copepods	1.47	11.9	0.70	8.8	0.26	7.4
Foraminifera	0.99	8.0	1.01	12.6	1.21	34.7
Polychaetes	0.22	1.8	0.92	11.5	0.68	19.3
Others	0.49	3.9	0.07	0.9	0.02	0.5
Total	12.36	100.0	7.95	100.0	3.49	100.0

Nematoda (13.8%), and Arthropoda (13.2%). At Station 1°N, macrofaunal biomass was dominated by Arthropoda (76.8%), followed by Annelida (15.5%) and Nematoda (3.0%).

At Station 39°N, the highest macrofaunal abundance was observed in the 3–5 cm sediment layer (Fig. 6B). At Station 1°N, macrofaunal abundances were highest in the shallowest sediment layer (0–1 cm) (94 ± 54 ind. m^{-2}) and did not exceed 50 ind. m^{-2} on average at depths below 1 cm (Fig. 6B).

As reported in Amaro et al. (2019), mean megafaunal abundance was approximately 36-fold higher at Station 39°N (2144.4 ± 593.4 ind. ha^{-1}) than at Station 1°N (54.5 ± 27.4 ind. ha^{-1}). At both stations, holothurians were the dominant megafaunal group, accounting for 70.9 ± 26.3% and 67.7 ± 3.8% of total megafaunal abundance at stations 1°N and 39°N, respectively.

3.5. Isotopic compositions of meio-, macro-, and megafauna

C and N isotopic compositions of meio-, macro-, and megafauna were plotted together with those of surface sediments (Fig. 7). Overall, 2 holothurian species, 25 macrofaunal taxa, and 5 meiofaunal taxa were analyzed for their C and N isotopic compositions at Station 39°N. At Station 1°N, 3 holothurian species, 12 macrofaunal taxa, and 4 meiofaunal taxa were analyzed. At Station 12°N, only 2 meiofaunal taxa (nematodes and meiofaunal polychaetes) were examined for their C and N isotopic compositions (Supplementary Fig. 4).

The uppermost sediment layer (0–1 cm) of Station 39°N had C and N isotopic compositions of –20.8 and 7.0‰, respectively (Table 1). Those of macrofauna ranged from –26.2 to –17.1‰ for $\delta^{13}C$ and 4.0 to 15.3‰ for $\delta^{15}N$ (Fig. 7A). Holothurian samples exhibited almost identical $\delta^{13}C$ values ranging from –16.6 to –15.7‰, which were substantially higher than those of meio- and macrofauna. Among macrofauna, Sipuncula (Annelida), Orbiniidae (Annelida), Hesionidae (Annelida), and Nemertea exhibited higher $\delta^{15}N$ (14.5–15.3‰) than other taxa, while Sabelidae (Annelida), Cirratulidae (Annelida), Fauveliopsidae (Annelida), and Cumacea (Arthropoda) exhibited low $\delta^{15}N$ values (5.3–8.2‰). Meiofauna exhibited more variability in $\delta^{15}N$ values, varying from –3.5 to 15.5‰ (Fig. 7A). Foraminifera typically exhibited low $\delta^{15}N$ values (mean, –2.3 ± 1.5‰). Some polychaetes also exhibited low $\delta^{15}N$ values; other metazoan meiofauna, in general, exhibited isotopic compositions similar to those of macrofauna. Nematodes had the highest $\delta^{15}N$ values among metazoan meiofauna, with a mean of 11.8 ± 1.7‰. Desmoscolecida (a nematode taxon) exhibited a narrow range of $\delta^{15}N$ values (8.3 to 9.4‰), which was substantially lower than that of other nematodes. The $\delta^{15}N$ values of harpacticoid copepods (7.5 ± 1.7‰) was intermediate between foraminifera and nematodes. The $\delta^{13}C$ values of nematodes (–21.1 ± 0.7‰), Desmoscolecida nematodes (–22.0 ± 0.4‰), and harpacticoid copepods (–20.6 ± 0.8‰) were similar to that of the shallowest surface sediments (–20.8‰). The $\delta^{13}C$ values of foraminifera were also similar on average but had more variability (–20.2 ± 3.6‰).

At Station 1°N, the 0–1 cm sediment layer exhibited C and N isotopic compositions of –19.5‰ and 12.0‰, respectively (Table 1). The isotopic compositions of macrofauna ranged from –28.0 to –17.5‰ for $\delta^{13}C$ and

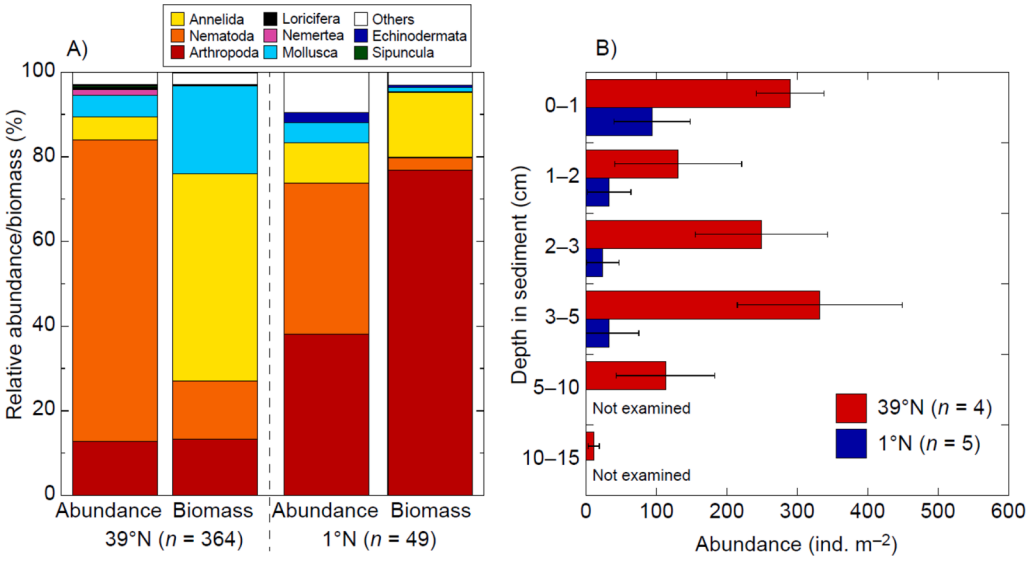

Fig. 6. Macrofaunal abundance and biomass at stations 39°N and 1°N. (A) Higher taxonomic composition of macrofauna in terms of abundance and biomass in natural background cores collected at stations 39°N (based on 364 individuals) and 1°N (based on 49 individuals). (B) Vertical profiles of total abundance (reported as individuals m^{-2} for each centimeter of sediment depth). Note that depths below 5 cm were not examined at Station 1°N. Error bars indicate standard deviations calculated from four (Station 39°N) and five (Station 1°N) replicate cores.

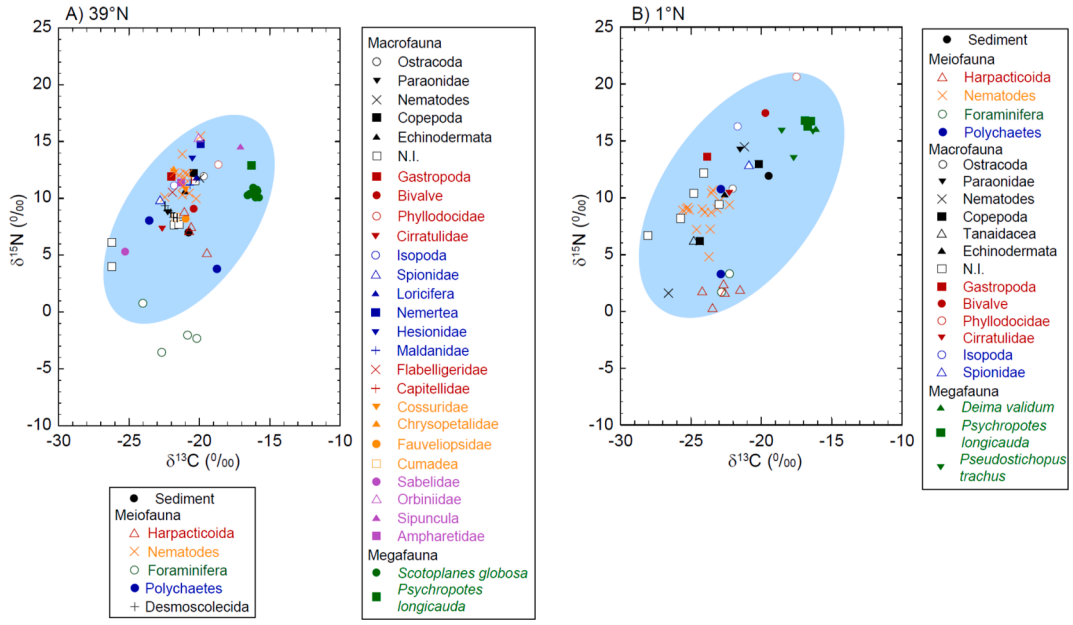

Fig. 7. Carbon and nitrogen isotopic compositions of holothurians, macrofauna, meiofauna, and surface sediments at stations 39°N and 1°N. Ranges of metazoan values (i.e. excluding foraminifera) are indicated as light blue ellipses at each station. (For interpretation of the references to colour in this figure legend, the reader is referred to the web version of this article.)

1.6 to 20.7‰ for $\delta^{15}N$ (Fig. 7B). The $\delta^{13}C$ values of holothurians *Deima validum* and *Psychropotes longicauda* were highest among the examined fauna. Among meio- and macrofauna, Phyllodocidae (Annelida), Bivalvia, and Isopoda (Arthropoda) exhibited high $\delta^{15}N$ values (16.3–20.7‰), and a Nematoda sample, Tanaidacea (Arthropoda), and Copepoda (Arthropoda) exhibited low $\delta^{15}N$ values (1.6–6.2‰). As was the case at Station 39°N, foraminifera collected at Station 1°N also exhibited low $\delta^{15}N$ values (1.7–3.3‰) (Fig. 7B, Supplementary Fig. 4). Harpacticoid copepods also exhibited low $\delta^{15}N$ values, but with considerable variability (range, 0.3–6.3‰) around a mean of 2.5 ± 2.2‰. Nematodes had substantially higher $\delta^{15}N$ than foraminifera and harpacticoid copepods (mean, 8.7 ± 1.5‰; range, 4.7–10.6‰). All meiofaunal $\delta^{15}N$ values were lower than that of the surface sediment (12.0‰). The $\delta^{13}C$ values of all examined taxa, namely, foraminifera (–22.8 to –22.3‰), harpacticoid copepods (–22.0 ± 2.3‰), nematodes (–24.0 ± 1.0‰), and meiofaunal polychaetes (–22.9‰), had similar ranges and were lower than that of surface sediments (–19.5‰).

At Station 12°N, the 0–1 cm sediment layer had C and N isotopic compositions of –19.5‰ and 9.8‰, respectively. As was the case at Station 1°N, both the $\delta^{13}C$ (–25.0 ± 0.6‰) and $\delta^{15}N$ (4.8 ± 1.8‰) values of nematodes were substantially lighter than that of surface sediments (Supplementary Fig. 4).

Overall, we observed a wider range of metazoan $\delta^{15}N$ (i.e., excluding foraminifera) at Station 1°N (1.6–20.7‰; Fig. 7B) than at Station 39°N (4.0–15.3‰; Fig. 7A), and a larger dispersion of values at Station 1°N (SD = 5.0‰) than at Station 39°N (SD = 3.1‰). The entire trophic levels of macro- and megafaunal organisms (assuming a ^{15}N enrichment factor of 3.4‰ with increasing trophic level; Minagawa and Wada, 1984) were 5.6 at Station 1°N and 3.3 at Station 39°N. The $\delta^{15}N$ and $\delta^{13}C$ values of benthic organisms, particularly macrofauna and megafauna, showed an overall trend that ranged between $\delta^{15}N/\delta^{13}C$ slope from 1.24 (Ohkouchi et al., 2015) to 1.6 (Wada et al., 2013).

4. Discussion

4.1. POC flux and abyssal benthic biota in sediments

The DOU rates (243.0, 46.6, and 18.9 μM O_2 m^{-2} d^{-1} at stations 39°N, 1°N, and 12°N, respectively) clearly showed enhanced OM mineralization rates at higher latitudes where higher POC fluxes are estimated. However, whereas the POC flux at Station 39°N was roughly 2 and 5 times higher than at stations 1°N and 12°N, respectively, DOU at Station 39°N was 5 and 13 times higher than at stations 1°N and 12°N, respectively. This suggests that the POC flux at Station 39°N contained a higher fraction of labile OM than at stations 1°N and 12°N. This is consistent with the high concentration of major biochemical OM components (i.e., carbohydrates, proteins, lipids, and pheopigments) in the sediment at Station 39°N. For instance, pheopigment concentrations in the 0–1 cm sediment layer were 1 to 2 orders of magnitude higher at Station 39°N than at stations 1°N and 12°N (Fig. 3), even though TOC concentrations at Station 39°N were similar to those at Station 1°N (Fig. 2a). Although carbohydrate and protein concentrations were also highest at Station 39°N, intermediate at Station 1°N, and lowest at Station 12°N (Supplementary Fig. 2, Table 2; Amaro et al., 2019), the differences between stations were less pronounced. Inconsistencies between TOC and labile OM concentrations have also been reported from a deep-sea bathymetric transect in the Eastern Mediterranean Sea (Danovaro et al., 1993) and Arctic Sea (Górska et al., 2020), indicating that the proportion of sediment TOC accounted for by labile OM differs greatly between oceanic settings. Meanwhile, labile OM contributes only < 5% of C demand of abyssal ecosystems (van Oevelen et al., 2012), highlighting the importance of studies on biodegradability of TOC in sediments.

Studies of the abyssal plain have identified strong linear relationships between POC flux and both the abundance and biomass of specific biotic size classes such as prokaryotes, macrofauna, and megafauna (Smith et al., 1997, 2008). In our study, we also observed a relationship between POC flux and both the abundance and biomass of the organisms studied; however, the impacts of POC fluxes differed among size classes. Differences in faunal and prokaryotic abundance between stations 39°N and 1°N were more evident for large organisms than for small ones (Figs. 4, 5, and 6; Amaro et al., 2019). At Station 39°N, megafaunal and macrofaunal abundances were 36 and 5.4 times higher, respectively, than at Station 1°N (Fig. 6; Amaro et al., 2019). Similarly, macrofaunal biomass at Station 39°N was 12 times higher than at Station 1°N. Meiofaunal abundance and biomass at Station 39°N were 3.5 and 1.6 times higher, respectively, than at Station 1°N (Fig. 5). Prokaryotic abundances at the two stations were, however, nearly equivalent

between the sites regardless of the difference in POC fluxes (Fig. 4).

In the deep-sea subseafloor sediments, microbial cell abundance is generally correlated with TOC concentration (Kallmeyer et al., 2012), and microbial cells are thought to have longer generation times in oligotrophic sediments (D'Hondt et al., 2009). In the abyssal surface sediments, Smith et al. (1997) also found a weak relationship between annual POC flux and bacterial biomass, and they suggested that the quicker turnover of microbes as compared to larger organisms means that their biomass is more closely correlated to shorter periods of POC flux before the sampling than to annual flux. In our study, although the prokaryotic cell abundance in the 0–1 cm sediment layer was similar among the three stations, higher viral abundances and higher VPR at Station 39°N were observed (Fig. 4). Viral production is depending on the activity of host microbes, and subsequent viral infection and production stimulates the activity of microbial ecosystem via viral shunt (Danovaro et al., 2008; Corinaldesi et al., 2012). The approximately 10-fold higher viral abundance and VPR at Station 39°N suggest the occurrence of higher turnover of prokaryotes than the other stations. Although caution should be applied when inferring direct relationships between VPR and microbial activity (Parikka et al., 2017; Cai et al., 2019; Manea et al., 2019), our geochemical observations (e.g., the high DOU and abundant labile OM) and the higher aminopeptidase enzymatic activities measured at Station 39°N are consistent with a more active microbial assemblage. These results suggest that the higher POC flux at Station 39°N might drive enhanced prokaryotic activity and turnover, possibly also accelerated by viral shunt and faster cycling of more labile OM. This would reconcile the apparent discrepancy between the similar prokaryotic cell abundances found in the shallowest sediment layer at the three stations and the evidence of higher cell metabolic activity at Station 39°N. An experimental study using isotopically labeled algae to stimulate benthic organisms at Station 39°N showed no substantial changes in prokaryotic cell numbers after 2 and 51 d, but there were significant increases in both bacterial enzymatic activities and viral production rates (H. Nomaki, unpublished results). This supports the above-mentioned hypothesis that higher POC flux can enhance prokaryotic cell metabolism. At the same time, viral infections and virus-induced cell lysis can accelerate prokaryotic turnover and limit overall cell abundance, possibly negating the effect of higher POC fluxes on the number of prokaryotic cells.

4.2. Vertical distributions of benthic organisms and OM

At Station 1°N, peaks in macrofaunal and meiofaunal abundances were observed in the 0–1 cm sediment layer, which also harbored most of the labile OM (Figs. 3 and 4). At Station 39°N, on the other hand, macro- and meiofaunal abundances in the 2–5 cm sediment layer were comparable to those in the 0–1 cm layer (Figs. 5 and 6). Similar vertical patterns were also observed in prokaryotic abundance. The vertical profiles reported above are similar to those of pheopigment concentrations (Fig. 3), with the difference being the existence of a subsurface pheopigment maximum at 10–15 cm at Station 39°N. The abundances of prokaryotes, viruses, nematodes, copepods, and total macrofauna were significantly correlated with Phe *a* and total pheopigment concentrations in the sediments (Table 5). At the same time, we found no significant correlations between the abundances of these biotic components and dissolved oxygen concentrations (Table 5). Meiofaunal vertical distributions in sediment have been reported to be controlled by oxygen penetration depths (Shirayama, 1984b), particularly in areas where OM concentrations are high and oxygen availability is confined to the top few millimeters of sediment (Jorissen et al., 1995). In the present study, oxygen penetration into the sediment was much shallower at Station 39°N than at stations 1°N and 12°N. Oxygen penetration was quite extensive at the oligotrophic stations (1°N and 12°N), with high sediment DO concentrations observed throughout the top 30 cm (Fig. 2b). Instead, food availability seemed to limit vertical distributions of fauna and prokaryotes.

Table 5
Correlations between prokaryotic cell numbers, viral abundances, meiofaunal and macrofaunal densities, and environmental parameters at different sediment depths. Correlations involving prokaryotes, viruses, and macrofauna were tested with data from stations 39°N and 1°N. Correlations involving meiofauna were tested using data from all three stations.

	Prokaryotes		Viruses		Nematodes		Copepods		Foraminifera		Macrofauna		Dissolved oxygen		Water content	
	r	*p*-value	*r*	*p*-value	*r*	*p*-value	*r*	*p*-value	*r*	*p*-value	*r*	*p*-value	*r*	*p*-value	*r*	*p*-value
*Prokaryotic cell numbers	–	–	0.89	<0.01	0.91	<0.05	0.50	n.s.	0.34	n.s.	0.95	<0.01	−0.45	n.s.	0.96	<0.001
*Viral abundances	0.89	<0.01	–	–	0.96	<0.01	0.69	n.s.	−0.10	n.s.	0.90	<0.01	−0.40	n.s.	0.96	<0.001
**Nematodes	0.90	<0.01	0.94	<0.001	–	–	0.87	<0.001	0.67	<0.05	0.96	<0.001	−0.52	n.s.	0.07	n.s.
**Copepods	0.61	n.s.	0.73	<0.05	0.87	<0.001	–	–	0.68	<0.05	0.69	n.s.	−0.13	n.s.	−0.03	n.s.
**Foraminifera	0.42	n.s.	0.09	n.s.	0.67	<0.05	0.68	<0.05	–	–	0.37	n.s.	−0.32	n.s.	−0.18	n.s.
**Total macrofauna	0.98	<0.001	0.94	<0.001	0.96	<0.001	0.69	n.s.	0.37	n.s.	–	–	−0.51	n.s.	0.96	<0.001
	NO_3^-		NO_2^-		NH_4^+		PO_4^{3-}		TOC		Total nitrogen		Phe *a*		Paeopigments	
	r	*p*-value	*r*	*p*-value	*r*	*p*-value	*r*	*p*-value	*r*	*p*-value	*r*	*p*-value	*r*	*p*-value	*r*	*p*-value
*Prokaryotic cell numbers	−0.53	n.s.	0.93	<0.001	0.58	n.s.	0.85	<0.01	0.74	<0.05	0.17	n.s.	0.94	<0.01	0.94	<0.01
*Viral abundances	−0.49	n.s.	0.83	<0.05	0.46	n.s.	0.88	<0.01	0.73	<0.05	0.08	n.s.	0.89	<0.01	0.87	<0.05
**Nematodes	−0.46	n.s.	0.95	<0.001	0.81	<0.01	0.88	<0.001	0.79	<0.01	0.73	<0.01	0.94	<0.001	0.94	<0.001
**Copepods	−0.10	n.s.	0.77	<0.01	0.83	<0.001	0.65	<0.05	0.72	<0.01	0.71	<0.01	0.74	<0.01	0.74	<0.01
**Foraminifera	−0.25	n.s.	0.68	<0.05	0.76	<0.01	0.46	n.s.	0.62	<0.05	0.65	<0.05	0.54	n.s.	0.55	n.s.
**Total macrofauna	−0.60	n.s.	0.96	<0.001	0.39	n.s.	0.95	<0.001	−0.26	n.s.	0.32	n.s.	0.96	<0.001	0.96	<0.001

* Examined to a depth of 10 cm.
** Examined to a depth of 5 cm.

Based on macrofaunal vertical distributions (Fig. 6) and sedimentological analysis at Station 39°N (K. Seike, unpublished results), sediment bioturbation by macrofauna down to a depth of approximately 10 cm could account for the penetration of labile OM into deeper sediment layers (Smith et al., 1996; Stephens et al., 1997). In situ experimental studies during which phytodetritus was added on the abyssal seafloor have shown that in the eutrophic North-East Atlantic, the benthic abyssal macrofauna rapidly reworked most of the added phytodetritus, while meiofauna and bacteria displayed a retarded response (Witte et al., 2003). Conversely, similar experiments conducted in the oligotrophic East Pacific Ocean showed that bacteria rather than macrofauna were early players in phytodetritus processing (Sweetman et al., 2018). As macrofauna relies on the availability of labile OM, the lower OM concentrations we found in the oligotrophic area (1°N) may explain why the macrofauna is confined to surface sediments in this area (i.e., the 0–1 cm depth layer). In turn, this could hamper sediment mixing by macrofauna and consequent OM delivery to the subsurface at 1°N. Conversely, the higher macrofauna abundance we found in the eutrophic area (39°N) (Fig. 6) may contribute to driving different patterns of OM processing in the two areas (Middelburg, 2018). In a parallel study, we conducted similar experiments involving phytodetritus addition to the sediments at the 39°N and 1°N areas. We observed rapid mixing of labelled algae to approximately 5 cm depth at Station 39°N after 1 d following the addition of phytodetritus, while no mixing deeper than 2–3 cm was detected at Station 1°N even after 2 months (H. Nomaki, unpublished results). These observations are consistent with the vertical distributions of labile OM at Stations 39°N and 1°N (Fig. 3), and support current evidence for the important role of macrofouna in sediment reworking at the seafloor (Middelburg, 2018).

In fact, we observed considerable mixing of labile OM into deeper sediment layers at Station 39°N, with high pheopigment concentrations persisting down to a depth of 15 cm (Fig. 3). Smith et al. (1996) measured pheopigment concentrations in equatorial Pacific abyssal sediments across a range of POC fluxes and found higher pheopigment concentrations at high POC flux stations. They even identified Chl *a* in deep sediment layers (at least 5 cm depth). However, the concentration profiles showed an exponential decrease of all analyzed pigment compounds, with a surface peak at all examined stations. By contrast, at Station 39°N, we measured high pheopigment concentrations down to a depth of 15 cm and observed abundant macrofauna, meiofauna, and prokaryote communities in subsurface layers (Figs. 4–6). This intense mixing, probably due to the high macrofaunal activities, appears an exception for abyssal plain ecosystems investigated so far. The macrofaunal effect on the burial into the sediment of labile OM deep may also reduce its oxidation with oxygenated bottom water. At Station 39°N, sedimentary protein concentrations are almost 2-fold higher than at other abyssal plains (i.e. the Porcupine Abyssal Plain; Amaro et al., 2019), and this high labile sediment OM is supported by a combination of high POC flux to the seafloor and rapid bioturbation by both macro- and megafauna (Jumars et al., 1990), as was observed abundantly at this station.

An interesting correlation was found between biotic components and sediment nitrite (NO_2^-) concentrations at the three stations (Table 5). This may result from the degradation of OM to produce ammonium and subsequent ammonia oxidation (Francis et al., 2007; Nunoura et al., 2013). In the presence of DO, nitrite concentrations may more closely represent amounts of mineralized OM *in situ* than other nutrients (e.g., nitrate, ammonium, and phosphate) that have complex pathways of production and consumptions. Further studies are required to fully understand the relationships between OM mineralization and nutrient concentrations in sediment pore water.

4.3. Natural isotopic compositions and food-web structures at stations 39°N and 1°N

The range of metazoan trophic levels (as inferred from $\delta^{15}N$) at the oligotrophic Station 1°N was broader than at the eutrophic Station 39°N (Fig. 7). In general, $\delta^{15}N$ increases ca. 3‰ from resources to consumers, although the exact values may vary among organisms and feeding habits (Vander Zanden and Rasmussen, 2001; McCutchan et al., 2003). As described above, entire trophic levels of the macro- and megafaunal food web were 5.6 and 3.3 at stations 1°N and 39°N, respectively, assuming a ^{15}N enrichment factor of 3.4‰ per trophic level (Minagawa and Wada 1984).

Water column zooplankton have a broader range of $\delta^{15}N$ in oligotrophic ecosystems than in eutrophic ecosystems in the western North Pacific (M. Aita-Noguchi, personal communication). These might be explained by differences in food availability and faunal biomass under different trophic conditions. In eutrophic ecosystems, where phytoplankton-derived OM is abundant, many heterotrophs can gain their nutrition directly from algae or phytodetritus. In contrast, in oligotrophic ecosystems, where phytoplankton OM is limited, only some organisms can gain their nutrition from phytodetritus. In this case, some heterotrophs are likely to develop different feeding habits that utilize refractory OM (Iken et al., 2001).

The high variability of $\delta^{15}N$ values at the oligotrophic Station 1°N may also be explained by differences in the size of primary producers and the contribution of small heterotrophs that graze small algae. In the oligotrophic ocean, surface primary producers are dominated by small (<2 μm) phytoplankton (Campbell et al., 1994, 1997). This potential food source is largely unavailable to large zooplankton due to size-constraints on feeding mechanisms (e.g. Gonçalves et al., 2014). In such ecosystems, small heterotrophs, including protists, directly consume picoplankton and help transfer nutrients to higher trophic levels (Calbet and Landry, 1999; Calbet and Saiz, 2005). By contrast, in eutrophic areas where primary producers are dominated by large algae such as diatoms, zooplankton can consume the algae directly. Consequently, surface water ecosystems in the oligotrophic ocean have more trophic levels than in the eutrophic ocean. At the abyssal plain, POM is derived from the surface ocean in the form of phytodetritus (i.e., aggregates of phytoplankton that incorporate zooplankton carcasses, and prokaryotes) (Beaulieu 2002). Therefore, the size effects of primary producers at the ocean surface may be obscured in abyssal food webs. However, diatom or cyanobacteria cells with intact structures have sometimes been identified in phytodetritus (Thiel et al., 1989; Beaulieu and Smith, 1998). Reports that some small heterotrophs such as foraminifera selectively ingest diatoms and green algae from sediments (Nomaki et al., 2006) suggest that the size of primary producers in the ocean surface may also play a role in determining the number of trophic levels. Shifts in phytoplankton assemblages from large cells to picoplankton, which are predicted to result from global climate change and ocean warming, could also alter abyssal food-web structures and hence biogeochemical cycles (Moran et al., 2010; Flombaum et al., 2013; Pörtner et al., 2014).

Interestingly, $\delta^{13}C$ also showed broad ranges at each station. This was particularly true for macrofauna, which had $\delta^{13}C$ values ranging from –26.2 to –17.1‰ at Station 39°N and –28.0 to –17.5‰ at Station 1°N. Surface sediment $\delta^{13}C$ values were –20.8‰ and –19.5‰ at stations 39°N and 1°N, respectively, which are on the intermediate or slightly heavier end of the macrofaunal $\delta^{13}C$ range. This may indicate that the sediment contains a variety of organisms and OM with different $\delta^{13}C$, and selective feeding on particular organisms can create a broad range of $\delta^{13}C$ values (Michel et al., 2016; Mincks et al., 2008). For example, amino acid compositions differ among organisms, and the $\delta^{13}C$ of individual amino acids can differ by over 30‰ even within a single organism (Sun et al., 2020). Selective ingestion or assimilation and digestion of OM within sediments should produce a range of $\delta^{13}C$ values. Compound-specific isotope analyses may shed light on these complex food webs that include a variety of food sources (Chikaraishi et al., 2009; Ishikawa, 2018; Ishikawa et al., 2018).

We measured the isotopic compositions of individual holothurian samples rather than the mean for a taxon (as opposed to all of the

meiofaunal and some of the macrofaunal samples, for which we used a mixture of tens to hundreds of specimens). Nevertheless, holothurians (e.g. *Scotoplanes globosa* at Station 39°N and *Psychropotes longicauda* at Station 1°N) had a narrow range of $\delta^{13}C$ and $\delta^{15}N$ values at both stations (Fig. 7, Amaro et al., 2019). This may reflect their feeding habits, with different specimens ingesting similar food sources. Deep-sea holothurians are commonly surface deposit feeders that feed on surface sediment, which usually contains more labile OM than subsurface layers (Amaro et al., 2015, 2019). By ingesting a sufficient area of the sea floor during the period reflected in their tissue isotopic compositions (which is determined by the rate of isotopic turnover), different specimens may share similar isotopic compositions due to the averaging of heterogeneous OM sources in surface sediments. By contrast, deep-sea predators and scavengers are more likely to have fed on only a few prey items during a similar period, contributing to high isotopic variability among individuals of the same taxon. Further studies are needed to examine relationships between $\delta^{13}C$ variability and the feeding habits of each species.

Some meiofauna had $\delta^{15}N$ values that were substantially lower than that of phytoplankton in the surface ocean of the western North Pacific (Noguchi and Wada, 2017). This was especially true for foraminifera, which had $\delta^{15}N$ ranges of 1.7 and 3.3‰ at Station 1°N and –3.5 to 0.8‰ at Station 39°N. Foraminifera, particularly agglutinated species, are known to sometimes have wide $\delta^{15}N$ ranges (Iken et al., 2001; Jeffreys et al., 2015). On the Pakistan margin, agglutinated monothalamids exhibited $\delta^{15}N$ values as low as –5‰ in the oxygen minimum zone and at shallower depths (Jeffreys et al., 2015). Low $\delta^{15}N$ values (ca. 0‰) are also observed in the Oman margin, and Jeffreys et al. (2015) speculate that these low values reflect the utilization of ^{15}N-depleted inorganic N resulting from incomplete organic N mineralization. The main group of foraminifera examined in our study, the monothalamids, may take up ^{15}N-depleted inorganic N by adsorption onto mineral particles in their agglutinated walls. Abyssal monothalamids typically contain stercomata (Gooday et al., 2008, 2018), which also contain clay minerals and thus possible to adsorb ^{15}N-depleted inorganic N. In this study, the $\delta^{15}N$ values of monothalamids may reflect that of inorganic N attached to mineral particles in the tests or stercomata. This is consistent with the low C:N ratios (i.e., high N content relative to C) of agglutinated foraminifera in our study (range, 2.9–3.7), which differed considerably from those of bathyal calcareous foraminifera (range, 4.3–6.2 with the exception of *Chilostomella ovoidea*; Nomaki et al., 2008).

5. Conclusions

In this study, we demonstrated that the eutrophic abyssal plain at Station 39°N (in eutrophic condition) is characterized by higher labile OM concentrations, benthic faunal abundance and oxygen uptake rates, than those at lower latitudes (Stations 1°N and 12°N) in oligotrophic and ultra-oligotrophic conditions, which showed low POC fluxes. The abundance of large organisms varied considerably among stations, but that of small eukaryotes and prokaryotes varied less, likely due to the faster turnover of small-sized organisms. The high megafaunal and macrofaunal abundances in the high-POC-flux station caused the intense sediment mixing and consequent burial of labile OM, allowing small heterotrophic eukaryotes and prokaryotes to penetrate in deeper sediment layers. The food-web structure of the abyssal plains was controlled not only by the amount of POC flux, but also by size of the primary producers. Our study of emphasizes the importance of POC flux and particle features in driving the abundance, diversity, and functions of abyssal ecosystems.

Declaration of Competing Interest

The authors declare that they have no known competing financial interests or personal relationships that could have appeared to influence the work reported in this paper.

Acknowledgements

This research was supported by Marie Skłodowska-Curie Actions through the project CEFMED [project number 327488] and by JSPS KAKENHI [grant numbers 24540504, JP16K00534, and JP19K04048]. We thank the onboard scientists, officers, and crews of the R/V *Yokosuka* and the manned submersible *Shinkai 6500* for their help during the cruises. We also thank Sachie Sugime, Yuki Iwadate, and Kaya Oda for their help on meiofaunal analyses and isotope sample preparation. We thank to the two anonymous reviewers and the editors, who provided helpful comments on an earlier version of this manuscript.

Appendix A. Supplementary material

Supplementary data to this article can be found online at https://doi.org/10.1016/j.pocean.2021.102591.

References

Amaro, T., de Stigter, H., Lavaleye, M., Duineveld, G., 2015. Organic matter enrichment in the Whittard Channel (northern Bay of Biscay margin, NE Atlantic); its origin and possible effects on benthic megafauna. Deep-Sea Res. Pt. I 102, 90–100.
Amaro, T., Rastelli, E., Matsui, Y., Danovaro, R., Wolff, G.A., Nomaki, H., 2019. Possible links between the holothurian lipid compositions to differences in organic matter (OM) supply at the western Pacific abyssal plains. Deep-Sea Res. Pt. I 152, 103085.
Barry, J.P., Lovera, C., Buck, K.R., Peltzer, E.T., Taylor, J.R., Walz, P., Whaling, P.J., Brewer, P.G., 2014. Use of a free ocean CO_2 enrichment (FOCE) system to evaluate the effects of ocean acidification on the foraging behavior of a deep-sea urchin. Environ. Sci. Technol. 48, 9890–9897.
Beaulieu, S.E., 2002. Accumulation and fate of phytodetritus on the seafloor. Oceanogr. Mar. Biol. 40, 171–232.
Beaulieu, S.E., Smith Jr, K.L., 1998. Phytodetritus entering the benthic boundary layer and aggregated on the sea floor in the abyssal NE Pacific: macro- and microscopic composition. Deep-Sea Res. Pt. II 45, 781–815.
Billett, D.S.M., Lampitt, R.S., Rice, A.L., Mantoura, R.F.C., 1983. Seasonal sedimentation of phytoplankton in the deep-sea benthos. Nature 302, 520–522.
Billett, D.S.M., Bett, B.J., Reid, W.D.K., Boorman, B., Priede, M., 2010. Long-term change in the abyssal NE Atlantic: the 'Amperima Event' revisited. Deep-Sea Res. Pt. II 57, 1406–1417.
Billett, D.S.M., Bett, B.J., Rice, A.L., Thurston, M.H., Galeron, J., Sibuet, M., Wolff, G.A., 2001. Long-term change in the megabenthos of the Porcupine Abyssal Plain (NE Atlantic). Progr. Oceanogr. 50, 325–348.
Buesseler, K.O., Lamborg, C.H., Boyd, P.W., Lam, P.J., Trull, T.W., Bidigare, R.P., Bishop, J.K.B., Casciotti, K.L., Dehairs, F., Elskens, M., Honda, M., Karl, D.M., Siegel, D.A., Silver, M.W., Steinberg, D.K., Valdes, J., Van Mooy, B., Wilsoz, S., 2007. Revisiting carbon flux through the Ocean's twilight zone. Science 316, 567.
Cai, L., Jørgensen, B.B., Suttle, C.A., He, M., Cragg, B.A., Jiao, N., Zhang, R., 2019. Active and diverse viruses persist in the deep sub-seafloor sediments over thousands of years. ISME J. 13, 1857–1864.
Calbet, A., Landry, M.R., 1999. Mesozooplankton influences on the microbial food web: direct and indirect trophic interactions in the oligotrophic open ocean. Limnol. Oceanogr. 44, 1370–1380.
Calbet, A., Saiz, E., 2005. The ciliate-copepod link in marine ecosystems. Aquat. Microb. Ecol. 38, 157–167.
Campbell, L., Nolla, H.A., Vaulot, D., 1994. The importance of Prochlorococcus to community structure in the central North Pacific Ocean. Limnol. Oceanogr. 39, 954–961.
Campbell, L., Liu, H., Nolla, H.A., Vaulot, D., 1997. Annual variability of phytoplankton and bacteria in the subtropical North Pacific Ocean at Station ALOHA during the 1991–1994 ENSO event. Deep-Sea Res. Pt. I 14, 167–192.
Chiba, S., Saito, H., Fletcher, R., Yogi, T., Kano, M., Miyagi, S., Ogido, M., Fujikura, K., 2018. Human footprint in the abyss: 30 year records of deep-sea plastic debris. Mar. Policy 96, 204–212.
Chikaraishi, Y., Ogawa, N.O., Kashiyama, Y., Takano, Y., Suga, H., Tomitani, A., Miyashita, H., Kitazato, H., Ohkouchi, N., 2009. Determination of aquatic food-web structure based on compound-specific nitrogen isotopic composition of amino acids. Limnol. Oceanogr. Methods 7, 740–750.
Corinaldesi, C., Dell'Anno, A., Danovaro, R., 2012. Viral infections stimulate the metabolism and shape prokaryotic assemblages in submarine mud volcanoes. ISME J. 6, 1250–1259.
Danovaro, R., Fabiano, M., Croce, N.D., 1993. Labile organic material and microbial biomasses in deep-sea sediments (Eastern Mediterranean Sea). Deep Sea Res. 40, 953–965.
Danovaro, R., 2010. Methods for the study of deep-sea sediments, their functioning and biodiversity. CRC Press, New York.
Danovaro, R., Corinaldesi, C., Dell'Anno, A., Snelgrove, P.V., 2017. The deep-sea under global change. Curr. Biol. 27, R461–R465.
Danovaro, R., Dell'Anno, A., Corinaldesi, C., Magagnini, M., Noble, R., Tamburini, C., Weinbauer, M., 2008. Major viral impact on the functioning of benthic deep-sea ecosystems. Nature 454, 1084.

Danovaro, R., Fanelli, E., Aguzzi, J., Billett, D., Carugati, L., Corinaldesi, C., Dell'Anno, A., Gjerde, K., Jamieson, A.J., Kark, S., McClain, C., Levin, L.A., Levin, N., Ramirez-Llodra, E., Ruhl, H., Smith, C.R., Snelgrove, P.V.R., Thomsen, L., Van Dover, C.L., Yasuhara, M., 2020. Ecological variables for developing a global deep-ocean monitoring and conservation strategy. Nat. Ecol. Evol. 4, 181–192.

D'Hondt, S., Spivack, A.J., Pockalny, R., Ferdelman, T.G., Fischer, J.P., Kallmeyer, J., Abrams, L.J., Smith, D.C., Graham, D., Hasiuk, F., Schrum, H., Stancin, A.M., 2009. Subseafloor sedimentary life in the South Pacific Gyre. P. Natl. Acad. Sci. USA 106, 11651–11656.

Durden, J.M., Bett, B.J., Jones, D.O.B., Huvenne, V.A.I., Ruhl, H.A., 2015. Abyssal hills – hidden source of increased habitat heterogeneity, benthic megafaunal biomass and diversity in the deep sea. Progr. Oceanogr. 137, 209–218.

Flombaum, P., Gallegos, J.L., Gordillo, R.A., Rincón, J., Zabala, L.L., Jiao, N., Karl, D.M., Li, W.K.W., Lomas, M.W., Veneziano, D., Vera, C.S., Vrugt, J.A., Martiny, A.C., 2013. Present and future global distributions of the marine Cyanobacteria *Prochlorococcus* and *Synechococcus*. P. Natl. Acad. Sci. USA 110, 9824–9829.

Francis, C.A., Beman, J.M., Kuypers, M.M.M., 2007. New processes and players in the nitrogen cycle: the microbial ecology of anaerobic and archaeal ammonia oxidation. ISME J. 1, 19–27.

Giere, O., 2009. Meiobenthology. The microscopic motile fauna of aquatic sediments, second ed. Universität Hamburg, Hamburg.

Giordani, P., Helder, W., Koning, E., Miserocchi, S., Danovaro, R., Malaguti, A., 2002. Gradients of benthic–pelagic coupling and carbon budgets in the Adriatic and Northern Ionian Sea. J. Mar. Syst. 33, 365–387.

Goineau, A., Gooday, A.J., 2017. Novel benthic foraminifera are abundant and diverse in an area of the abyssal equatorial Pacific licensed for polymetallic nodule exploration. Sci. Rep. 7. Article 45288.

Gonçalves, R.J., van Someren Gréve, H., Couespel, D., Kiørboe, T., 2014. Mechanisms of prey size selection in a suspension-feeding copepod, *Temora longicornis*. Mar. Ecol. Prog. Ser. 517, 61–74.

Gooday, A.J., Nomaki, H., Kitazato, H., 2008. Modern deep-sea benthic foraminifera: a brief review of their morphology-based biodiversity and trophic diversity. Geol. Soc. Lond. Spec. Publ. 303, 97–119.

Gooday, A.J., Sykes, D., Góral, T., Zubkov, M.V., Glover, A.G., 2018. Micro-CT 3D imaging reveals the internal structure of three abyssal xenophyophore species (Protista, Foraminifera) from the eastern equatorial Pacific Ocean. Sci. Rep. 8. Article 12103.

Górska, B., Soltwedel, T., Schewe, I., Włodarska-Kowalczuk, M., 2020. Bathymetric trends in biomass size spectra, carbon demand, and production of Arctic benthos (76–5561 m, Fram Strait). Progr. Oceanogr. 186, 102370.

Hiraoka, S., Hirai, M., Matsui, Y., Makabe, A., Minegishi, H., Tsuda, M., Juliarni, Rastelli, E., Danovaro, R., Corinaldesi, C., Kitahashi, T., Tasumi, E., Nishizawa, M., Takai, K., Nomaki, H., Nunoura, T., 2020. Microbial community and geochemical analyses of trans-trench sediments for understanding the roles of hadal environments. ISME J. 14, 740–756. https://doi.org/10.1038/s41396-019-0564-z.

Iken, K., Brey, T., Wand, U., Voigt, J., Junghans, P., 2001. Food web structure of the benthic community at the Porcupine Abyssal Plain (NE Atlantic): a stable isotope analysis. Progr. Oceanogr. 50, 383–405.

Ishikawa, N.F., 2018. Use of compound-specific nitrogen isotope analysis of amino acids in trophic ecology: assumptions, applications, and implications. Ecol. Rese. 33, 825–837.

Ishikawa, N.F., Chikaraishi, Y., Takano, Y., Sasaki, Y., Takizawa, Y., Tsuchiya, M., Tayasu, I., Nagata, T., Ohkouchi, N., 2018. A new analytical method for determination of the nitrogen isotopic composition of methionine: Its application to aquatic ecosystems with mixed resources. Limnol. Oceanogr.: Methods 16, 607–620.

Jeffreys, R.M., Fisher, E.H., Gooday, A.J., Larkin, K.E., Billett, D.S.M., Wolff, G.A., 2015. The trophic and metabolic pathways of foraminifera in the Arabian Sea: evidence from cellular stable isotopes. Biogeosciences 12, 1781–1797.

Jorissen, F.J., de Stigter, H.C., Widmark, J.G.V., 1995. A conceptual model explaining benthic foraminiferal microhabitats. Mar. Maicropal. 26, 3–15.

Jumars, P., Mayer, L., Deming, J., Baross, J., Wheatcroft, R., 1990. Deep-sea deposit-feeding strategies suggested by environmental and feeding constraints. Philos. Trans. R. Soc. A 331, 85–101.

Kallmeyer, J., Pockalny, R., Adhikari, R.R., Smith, D.C., D'Hondt, S., 2012. Global distribution of microbial abundance and biomass in subseafloor sediment. P. Natl. Acad. Sci. USA 109, 16213–16216.

Laureman, L.M.L., Kaufmann, R.S., Smith, K.L., 1996. Distribution and abundance of epibenthic megafauna at a long time-series station in the abyssal NE Pacific. Deep-Sea Res. 43, 1075–l 104.

Lutz, M.J., Caldeira, K., Dunbar, R.B., Behrenfeld, M.J., 2007. Seasonal rhythms of net primary production and particulate organic carbon flux to depth describe the efficiency of biological pump in the global ocean. J. Geophys. Res. 112, C10011.

Manea, E., Dell'Anno, A., Rastelli, E., Tangherlini, M., Nunoura, T., Nomaki, H., Danovaro, R., Corinaldesi, C., 2019. Viral infections boost prokaryotic biomass production and organic C cycling in hadal trench sediments. Front. Microbiol. 10. Article 1952.

McCutchan, J.H., Lewis, W.M., Kendall, C., McGrath, C.C., 2003. Variation in trophic shift for stable isotope ratios of carbon, nitrogen, and sulfur. Oikos 102, 378–390.

Michel, L., David, B., Dubois, P., Lepoint, G., De Ridder, C., 2016. Trophic plasticity of Antarctic echinoids under contrasted environmental conditions. Polar Biol. 39, 913–923.

Middelburg, J.J., 2018. Reviews and syntheses: to the bottom of carbon processing at the seafloor. Biogeosciences 15, 413–427.

Minagawa, M., Wada, E., 1984. Stepwise enrichment of ^{15}N along food chains: further evidence and the relation between δ^{15}N and animal age. Geochim. Cosmochim. Acta 48, 1135–1140.

Mincks, S.L., Smith, C.R., Jeffreys, R.M., Sumida, P.Y.G., 2008. Trophic structure on the West Antarctic Peninsula shelf: Detritivory and benthic inertia revealed by δ^{13}C and δ^{15}N analysis. Deep-Sea Res. Pt. II 55, 2502–2514.

Moran, X.A., Lopez-Urrutia, A., Calvo-Diaz, A., Li, W.K.M., 2010. Increasing importance of small phytoplankton in a warmer ocean. Glob. Chang. Biol. 16, 1137–1144.

Naeher, S., Suga, H., Ogawa, N.O., Takano, Y., Schubert, C.J., Grice, K., Ohkouchi, N., 2016. Distributions and compound-specific isotopic signatures of sedimentary chlorins reflect the composition of photoautotrophic communities and their carbon and nitrogen sources in Swiss lakes and the Black Sea. Chem. Geol. 443, 198–209.

Noguchi, A.M., Wada, E., 2017. Tracing marine ecosystem dynamics and biogeochemical cycles using stable isotope ratios. Kaiyo Monthly 49, 430–436.

Nomaki, H., Heinz, P., Nakatsuka, T., Shimanaga, M., Ohkouchi, N., Ogawa, N.O., Kogure, K., Ikemoto, E., Kitazato, H., 2006. Different ingestion patterns of ^{13}C-labeled bacteria and algae by deep-sea benthic foraminifera. Mar. Ecol. Progr. Ser. 310, 95–108.

Nomaki, H., Ogawa, N.O., Ohkouchi, N., Suga, H., Toyofuku, T., Shimanaga, M., Nakatsuka, T., Kitazato, H., 2008. Benthic foraminifera as trophic links between phytodetritus and benthic metazoans: carbon and nitrogen isotopic evidence. Mar. Ecol. Progr. Ser. 357, 153–164.

Nomaki, H., Mochizuki, T., Kitahashi, T., Nunoura, T., Arai, K., Toyofuku, T., Tanaka, G., Shigeno, S., Tasumi, E., Fujikura, K., Watanabe, S., 2016. Effects of mass sedimentation event after the 2011 off the Pacific coast of Tohoku Earthquake on benthic prokaryotes and meiofauna inhabiting the upper bathyal sediments. J. Oceanogr. 72, 113–128.

Nomaki, H., Uejima, Y., Ogawa, N.O., Yamane, M., Watanabe, H.K., Senokuchi, R., Bernhard, J.M., Kitahashi, T., Miyairi, Y., Yokoyama, Y., Ohkouchi, N., Shimanaga, M., 2019. Nutritional sources of meio- and macrofauna at hydrothermal vents and adjacent areas: natural-abundance radiocarbon and stable isotope analyses. Mar. Ecol. Progr. Ser. 622, 49–65.

Nunoura, T., Nishizawa, M., Kikuchi, T., Tsubouchi, T., Hirai, M., Koide, O., Miyazaki, J., Hirayama, H., Koba, K., Takai, K., 2013. Molecular biological and isotopic biogeochemical prognoses of the nitrification-driven dynamic microbial nitrogen cycle in hadopelagic sediments. Environ. Microbiol. 15, 3087–3107.

Ogawa, N.O., Nagata, T., Kitazato, H., Ohkouchi, N., 2010. Ultra-sensitive elemental analyzer/isotope ratio mass spectrometer for stable nitrogen and carbon isotope analyses. In: Ohkouchi, N., Tayasu, I., Koba, K. (Eds.), Earth, life and isotopes. Kyoto University Press, Kyoto, pp. 339–353.

Ohkouchi, N., Ogawa, N.O., Chikaraishi, Y., Tanaka, H., Wada, E., 2015. Biochemical and physiological bases for the use of carbon and nitrogen isotopes in environmental and ecological studies. Prog. Earth Planet Sci. 2, 1.

Parikka, K.J., Le Romancer, M., Wauters, N., Jacquet, S., 2017. Deciphering the virus-to-prokaryote ratio (VPR): insights into virus–host relationships in a variety of ecosystems. Biol. Rev. 92, 1081–1100.

Paull, C.K., Greene, H.G., Ussler III, W., Mitts, P.J., 2002. Pesticides as tracers of sediment transport through Monterey Canyon. Geo-Mar. Lett. 22, 121–126.

Pörtner, H.O., Karl, D.M. Boyd, P.W., Cheung, W.W.L., Lluch-Cota, S.E,. Nojiri, Y., Schmidt, D.N., Zavialov, P.O., 2014. Ocean systems. In: Barros, C.B., Dokken, V.R., Mach, D.J., Mastrandrea, K.J., Bilir, M.D., Chatterjee, T.E., Ebi M.K.L., Estrada, Y.O., Genova, R.C., Girma, B., Kissel, E.S., Levy, A.N., MacCracken, S., Mastrandrea, P.R., White L.L. (Eds.), Climate Change 2014: Impacts, Adaptation, and Vulnerability. Part A: Global and Sectoral Aspects. Contribution of Working Group II to the Fifth Assessment Report of the Intergovernmental Panel on Climate Change. Cambridge University Press, Cambridge, United Kingdom and New York, NY, USA, pp. 411–484 (Field).

Ramirez-Llodra, E., Tyler, P.A., Baker, M.C., Bergstad, O.A., Clark, M.R., Escobar, E., Levin, L.A., Menot, L., Rowden, A., Smith, C.R., Van Dover, C.L., 2011. Man and the Last Great Wilderness: Human Impact on the Deep Sea. PLoS ONE 6, e22588.

Ruhl, H.A., 2007. Abundance and size distribution dynamics of abyssal epibenthic megafauna in the northeast Pacific. Ecology 88, 1250–1262.

Ruhl, H.A., Smith, K.L., 2004. Shifts in deep-sea community structure linked to climate and food supply. Science 305, 513–515.

Schlining, K., von Thun, S., Kuhnz, L., Schlining, B., Lundstern, L., Stout, N.J., Chaney, L., Connor, J., 2013. Debris in the deep: Using a 22-year video annotation database to survey marine litter in Monterey Canyon, central California, USA. Deep-Sea Res. Pt. I 79, 96–105.

Shirayama, Y., 1984a. The abundance of deep sea meiobenthos in the Western Pacific in relation to environmental factors. Oceanol. Acta 7, 113–121.

Shirayama, Y., 1984b. Vertical distribution of meiobenthos in the sediment profile in bathyal, abyssal and hadal deep sea systems of the Western Pacific. Oceanol. Acta 7, 123–129.

Smith, C.R., Hoover, D.J., Doan, S.E., Pope, R.H., DeMaster, D.J., Dobbs, F.C., Altabet, M. A., 1996. Phytodetritus at the abyssal seafloor across 10° of latitude in the central equatorial Pacific. Deep-Sea Res. Pt. II 43, 1309–1338.

Smith, C.R., Berelson, W., Demaster, J.D., Dobbs, F.C., Hammond, D., Hoover, D.J., Pope, R.H., Stephens, M., 1997. Latitudinal variations in benthic processes in the abyssal equatorial Pacific: control by biogenic particle flux. Deep-Sea Res. Pt. II 44, 2295–2317.

Smith, C.R., De Leo, F.C., Bernardino, A.F., Sweetman, A.K., Pedro Martinez, A., 2008. Abyssal food limitation, ecosystem structure and climate change. Trends Ecol. Evol. 23, 518–528.

Smith, K.L., Baldwin, R.J., Ruhl, H.A., 2006. Climate effect on food supply to depths greater than 4000 meters in the northeast Pacific. Limnol. Oceanog. 51, 166–176.

Smith, K.L., Ruhl, H.A., Bett, B., Billett, D.S.M., Lampitt, R.S., Kaufmann, R.S., 2009. Climate, carbon cycling, and deep-ocean ecosystems. P. Natl. Acad. Sci. USA 106, 19211–19218.

Smith, K.L., Ruhl, H.A., Kahru, M., Huffard, C.L., Shrman, A.D., 2013. Deep ocean communities impacted by changing climate over 24 y in the abyssal northeast Pacific Ocean. P. Natl. Acad. Sci. USA 110, 19838–19841.
Smith, K.L., Huffard, C.L., Ruhl, H.A., 2020. Thirty-year time series study at a station in the abyssal NE Pacific: An introduction. Deep-Sea Res. Pt. II 173, 104764.
Sonnewald, M., Dutkiewicz, S., Hill, C., Forget, G., 2020. Elucidating ecological complexity: Unsupervised learning determines global marine eco-provinces. Sci. Adv. 6, eaay4740.
Stefanoudis, P.V., Bett, B.J., Gooday, A.J., 2016. Abyssal hills: Influence of topography on benthic foraminiferal assemblages. Progr. Oceanogr. 148, 44–55.
Stephens, M.P., Kadko, D.C., Smith, C.R., Latasa, M., 1997. Chlorophyll-*a* and pheopigments as tracers of labile organic carbon at the central equatorial Pacific seafloor. Geochim. Cosmochim. Acta 61, 4605–4619.
Sun, Y., Ishikawa, N.F., Ogawa, N.O., Kawahata, H., Takano, Y., Ohkouchi, N. 2020. A method for stable carbon isotope measurement of underivatized individual amino acids by multi-dimensional high-performance liquid chromatography and elemental analyzer/isotope ratio mass spectrometry. Rapid Commun. Mass Spectr. doi: 10.1002/rcm.8885.
Sweetman, A.K., Smith, C.R., Shulse, C.N., Maillot, B., Lindh, M., Church, M.J., Meyer, K. S., van Oevelen, D., Stratmann, T., Gooday, A.J., 2018. Key role of bacteria in the short-term cycling of carbon at the abyssal seafloor in a low particulate organic carbon flux region of the eastern Pacific Ocean. Limnol. Oceanogr. 64, 694–713.
Thiel, H., Pfannkuche, O., Schriever, G., Lochte, K., Gooday, A.J., Hemleben, C., Mantoura, R.F.G., Turley, C.M., Patching, J.W., Riemann, F., 1989. Phytodetritus on the deep-sea floor in a central oceanic region of the Northeast Atlantic. Biol. Oceanogr. 6, 203–239.
Turley, C.M., Lochte, K., Lampitt, R.S., 1995. Transformations of biogenic particles during sedimentation in the northeastern Atlantic. Phil. Trans. R. Soc. Lond. B 348, 179–189.
Ullman, W.J., Aller, R.C., 1982. Diffusion coefficients in nearshore marine sediments. Limnol. Oceanogr. 27, 552–556.
Van Oevelen, D., Soetaert, K., Heip, C., 2012. Carbon flows in the benthic food web of the Porcupine Abyssal Plain: The (un)importance of labile detritus in supporting microbial and faunal carbon demands. Limnol. Oceanogr. 57, 645–664.
Vander Zanden, M.J., Rasmussen, J.B., 2001. Variation in $\delta^{15}N$ and $\delta^{13}C$ trophic fractionation: implications for aquatic food web studies. Limnol. Oceanogr. 46, 2061–2066.
Wada, E., Ishii, R., Aita, M.N., Ogawa, N.O., Kohzu, A., Hyodo, F., Yamada, Y., 2013. Possible ideas on carbon and nitrogen trophic fractionation of food cahins: a new aspect of food-chain stable isotope analysis in Lake Biwa, Lake Baikal, and the Mongolian grasslands. Ecol. Res. 28, 173–181.
Witte, U., Wenzhoefer, F., Sommer, S., Boetius, A., Heinz, P., Aberle, N., Sand, M., Cremer, A., Abraham, W.R., Jørgensen, B.B., Pfannkuche, O., 2003. In situ experimental evidence of the fate of a phytodetritus pulse at the abyssal sea floor. Nature 424, 763–766.
Zar, J.H., 2010. Biostatistical analysis, fifth ed. Prentice-Hall, New Jersey, p. 944.